7788–7805 Nucleic Acids Research, 2012, Vol. 40, No. 16 Published online 4 June 2012
doi:10.1093/nar/gks486

Quantitative proteomics profiling of the poly(ADP-ribose)-related response to genotoxic stress

Jean-Philippe Gagné[1], Émilie Pic[1], Maxim Isabelle[1], Jana Krietsch[1], Chantal Éthier[1], Éric Paquet[2], Isabelle Kelly[3], Michel Boutin[3], Kyung-Mee Moon[4], Leonard J. Foster[4] and Guy G. Poirier[1,*]

[1]Cancer Research Laboratory, [2]Genome Stability Laboratory, [3]Proteomics platform, Québec Genomic Center, Laval University - CHUQ Research Center, Québec, Canada G1V 4G2 and [4]Department of Biochemistry and Molecular Biology, University of British Columbia, Centre for High-Throughput Biology, Vancouver, British Columbia, Canada, V6T 1Z4

Received May 18, 2011; Revised May 1, 2012; Accepted May 3, 2012

ABSTRACT

Upon DNA damage induction, DNA-dependent poly(ADP-ribose) polymerases (PARPs) synthesize an anionic poly(ADP-ribose) (pADPr) scaffold to which several proteins bind with the subsequent formation of pADPr-associated multiprotein complexes. We have used a combination of affinity-purification methods and proteomics approaches to isolate these complexes and assess protein dynamics with respect to pADPr metabolism. As a first approach, we developed a substrate trapping strategy by which we demonstrate that a catalytically inactive Poly(ADP-ribose) glycohydrolase (PARG) mutant can act as a physiologically selective bait for the isolation of specific pADPr-binding proteins through its macrodomain-like domain. In addition to antibody-mediated affinity-purification methods, we used a pADPr macrodomain affinity resin to recover pADPr-binding proteins and their complexes. Second, we designed a time course experiment to explore the changes in the composition of pADPr-containing multiprotein complexes in response to alkylating DNA damage-mediated PARP activation. Spectral count clustering based on GeLC-MS/MS analysis was complemented with further analyses using high precision quantitative proteomics through isobaric tag for relative and absolute quantitation (iTRAQ)- and Stable isotope labeling by amino acids in cell culture (SILAC)-based proteomics. Here, we present a valuable resource in the interpretation of systems biology of the DNA damage response network in the context of poly(ADP-ribosyl)ation and provide a basis for subsequent investigations of pADPr-binding protein candidates.

INTRODUCTION

Poly(ADP-ribose) (pADPr) turnover is an important process involved in the transient response to DNA damage. The synthesis of pADPr that results from the activation of DNA-dependent poly(ADP-ribose) polymerases (PARPs) is one of the earliest step of DNA damage recognition and signaling in mammalian cells (1). During the response elicited by DNA damage, the addition of pADPr to chromatin-related proteins is associated with chromatin decondensation and dynamic nucleosome remodeling that tends to increase the accessibility of repair factors to DNA lesions (2). Numerous molecules are recruited at DNA- damage sites in a pADPr-dependent manner. Therefore, pADPr itself appears to be a signaling and scaffold molecule involved in the assembly of multi-subunit DNA repair complexes (3). In addition to covalent attachment of pADPr to target proteins, specific non-covalent pADPr interaction motifs have been characterized. Three major protein interaction modules were identified on the basis of their high affinity for pADPr: the macro domain (4), the poly(ADP-ribose)-binding zinc finger module (PBZ) (5) and the WWE domain (defined by the conserved residues tryptophan (WW) and glutamic acid (E)) that mediates protein–protein interactions in ubiquitin and ADP-ribose conjugation systems (6–8).

*To whom correspondence should be addressed. Tel: +1 418 654 2267; Fax: +1 418 654 2159; Email: guy.poirier@crchul.ulaval.ca

The authors wish it to be known that, in their opinion, the first two authors should be regarded as joint First Authors.

Besides domain-mediated interaction, several proteins are known to interact with pADPr through a generally short hydrophobic and basic region (9–11). This poly(ADP-ribose)-binding motif is widespread and frequently found in the DNA-binding domains of chromatin regulatory proteins and DNA repair factors. Collectively, pADPr-binding proteins generate a DNA repair network of protein factors through physical interactions with pADPr. In this view, pADPr behaves as a coordinator in the cellular response to genotoxic insults.

The macro domain has been the object of the first structural investigations on ADP-ribose recognition (12–13). A macroprotein was also used as a bait to define the ADP-ribosyl proteome, a method that proved to be effective although very limited gains in new protein identifications were achieved (14). A recent study from Slade and colleagues revealed that Poly(ADP-ribose) glycohydrolase (PARG) catalytic domain is a distant member of the ubiquitous ADP-ribose-binding macrodomain family (15). PARG is the main enzyme involved in the degradation of pADPr. Therefore, we reasoned that a catalytically inactive PARG mutant that forms stable interactions with pADPr, would also allow subsequent purification of poly(ADP-ribosyl)ated proteins and pADPr-containing protein complexes. A mass spectrometry (MS)-based substrate trapping strategy could further extent the proteome coverage achieved with antibody-mediated affinity-purification procedures. As part of this approach, we also revisited the strategy that couples affinity purification by an ADP-ribose-binding macrodomain (AF1521) with MS.

Over the past few years, our work, and that of many other labs exposed the fact that pADPr engages in highly specific non-covalent interactions with proteins (16–18). Strong binding to pADPr has the potential to act as a loading platform for a variety of proteins involved in DNA/RNA metabolism (19). Although pADPr-binding studies reflect the existence of strong molecular interactions with pADPr, it still remains a challenge to identify and quantify transient protein interaction with pADPr. The fast and transient dynamics of pADPr makes it an extremely challenging task. The use of DNA damaging agents that cause a broad spectrum of DNA lesions are useful tools to assess the modulation of the poly(ADP-ribosyl)ation reaction and the subsequent activation of DNA damage sensing enzymes.

N-methyl-N-nitro-N-nitrosoguanidine (MNNG) has been used for decades as an effective agent to induce massive pADPr synthesis through PARP-1 activation. In addition to inducing damage to the DNA bases, MNNG is an alkylating agent known to produce both DNA single-strand breaks (SSBs), as well as double-strand breaks (DSBs) (20,21). The exposure of cells to MNNG results in an almost immediate poly(ADP-ribosyl)ation of target proteins but little is known on their time course profiles, as well as their persistence in pADPr-containing protein complexes. As a first approach in this study, we used complementary proteome-mining methods that cover a large part of the accessible pADPr proteome. Using antibody-mediated and substrate trapping strategies to isolate pADPr-containing protein complexes, we present an overall picture of the pADPr proteome. Second, we focused on the highly dynamic composition of pADPr-containing protein complexes following an alkylation-induced DNA damage to provide insights into the functional processes modulated by poly(ADP-ribosyl)ation. The dynamic assembly of pADPr-containing protein complexes was revealed by the use of quantitative MS. Strategies for quantitative proteomic profiling included both *in vitro* and *in vivo* labeling approaches, as well as label-free quantitation. These proteome-wide approaches were coupled to pADPr affinity purification and complementary datasets were integrated and modeled for a more thorough insight into pADPr-binding protein dynamics. Here, we present the first quantitative proteomics investigation of the pADPr-associated proteome modulation in the context of DNA damage and PARP activation.

MATERIALS AND METHODS

Cell culture, vector construct and transfections

Human embryonic kidney 293 cells (HEK 293) and human cervical carcinoma cells (HeLa) were cultured (air/CO_2, 19:1, 37°C) in Dulbecco's modified Eagle's medium (DMEM) supplemented with 10% fetal bovine serum (FBS) (Hyclone-ThermoFisher Scientific, Ottawa, Canada). Penicillin (100 U/ml) and streptomycin (100 mg/ml) (Wisent, St-Bruno, Canada) were added to the culture media. Alkylating DNA damage was introduced using freshly prepared 100 µM MNNG for 5 min. Cells were washed twice with PBS before cell lysis or allowed to recover from the genotoxic insult for 1 or 2 h by replacing the growth medium with supplemented DMEM.

A human GFP-PARG-DEAD vector was modified by oligonucleotide-directed mutagenesis of the GFP-hPARG-110 (pEGFP-C1 expression vector, Clontech) previously described in Ref. (22). Mutagenic primers were made following the guidelines in the QuikChange® site-directed mutagenesis kit (Stratagene). A mutation was introduced at amino acid position 756 which completely abolishes PARG catalytic activity (E756D) as reported (23). Transfections were carried out with Effectene (Qiagen), as recommended by the manufacturer and cells were harvested 24 h post-transfection.

Immunoprecipitation of pADPr-containing protein complexes

HEK 293 and HeLa cells were seeded onto 150-mm cell culture dishes and grown up to 80–90% confluency (~15–20 millions cells/dish). Experiments were performed with cell extracts from three dishes per condition. Control cells were pre-incubated for 2 h with 5 µM PARP-1 inhibitor ABT-888 to maintain basal levels of pADPr, whereas a fast activation of PARP-1 resulting in a substantial increase in intracellular levels of pADPr was performed by incubating the cells with freshly prepared 100 µM MNNG for 5 min. All further steps were performed on ice or at 4°C. Two PBS washes were carried out prior to protein extraction with 2 ml/plate of lysis buffer [40 mM HEPES pH 7.5, 120 mM NaCl, 0.3% CHAPS, 1 mM

EDTA, 1X Complete™ protease inhibitor cocktail (Roche Applied Science, Indianapolis, IN, USA) and 1 μM PARG inhibitor ADP-HPD (adenosine 5′-diphosphate (hydroxymethyl) pyrrolidinediol) (EMD Chemicals, Gibbstown, NJ, USA)]. The whole cell lysates were pooled and placed on ice for 15 min and gently mixed for another 15–20 min on a rotating device for complete lysis. After homogenization, insoluble material was removed from the homogenate by centrifuging at 3000*g* for 5 min. Immunoprecipitation (IP) experiments were performed using magnetic Dynabeads™ covalently coupled to Protein G (Invitrogen, Burlington, Canada). The Dynabeads™ (125 μl/condition) were washed twice with 1 ml of 0.1 M sodium acetate buffer, pH 5.0 and coated with 12.5 μg of mouse monoclonal anti-pADPr antibody clone 10H (Tulip Biolabs, West Point, PA, USA), anti-GFP (Roche Applied Science, Indianapolis, IN, USA) or equivalent amount of normal mouse IgGs (Calbiochem-EMD Biosciences, San Diego, CA, USA). The antibody-coupled Dynabeads™ were incubated for 1 h with 1 ml of PBS containing 1% (w/v) bovine serum albumin (BSA) (Sigma-Aldrich, Oakville, Canada) to block non-specific antibody-binding sites. The beads were finally washed three times with 1 ml of lysis buffer and added to the pre-cleared pADPr-protein extract for a 2-h incubation with gentle mixing on a rotating device. Samples were washed five times with 10 ml of lysis buffer for 5 min. Protein complexes were eluted using 250 μl of 3X Laemmli sample buffer containing 5% β-mercaptoethanol and heated at 65°C for 5 min in a water bath. Proteins were resolved using 4–12% Criterion™ XT Bis–Tris gradient gel (Bio-Rad) and stained with Sypro Ruby (Bio-Rad) according to the manufacturer's instructions. Images were acquired using the Geliance CCD-based bioimaging system (PerkinElmer).

Isolation of pADPr-containing complexes using macrodomain pADPr affinity resin

pADPr-containing protein complexes were isolated with purified GST-Af1521 macrodomain fusion protein construct bound to glutathione beads (Tulip Biolabs, West Point, PA, USA). Macrodomain pADPr affinity resin was used essentially as described for IPs except that antibody-coupled magnetic beads are replaced with macrodomain affinity resin suspension (5 μl of the suspension/~1 ml of protein extract).

Estimation of pADPr levels after exposure to MNNG

The dynamics of pADPr was evaluated by a relative quantitation of pADPr levels in cells after exposure to MNNG (5 min) and following a recovery period (1 and 2 h). Control and MNNG-treated HEK 293 cells were washed with ice-cold PBS and fixed with a 4% formaldehyde solution in PBS for 15 min. Five PBS washes were performed before membrane permeabilization with a 0.5% Triton X-100 solution in PBS. Cells were washed three times with PBS and incubated for 90 min at room temperature with anti-pADPr monoclonal antibody clone 10H (Tulip BioLabs, West Point, PA, USA) diluted 1:1000 in PBS containing 2% FBS. PBS washes were performed before incubating cells with an AlexaFluor-488 anti-mouse secondary antibody (Invitrogen). Cells were washed with PBS and counterstained with Hoechst 33342. Fluoromount-G mounting media (Southern Biotechn, Birmingham, AL, USA) was used to prepare microscope slides. Immunofluorescence images were acquired on a Zeiss LSM510 META NLO laser scanning confocal microscope. Zen 2009 software version 5.5 SP1 (Zeiss) was used for image acquisitions and fluorescence intensity measurements. In total, 300 cell nuclei were analyzed from three independent experiments for each experimental condition (100 nuclei/condition). Relative fluorescence intensity was expressed in arbitrary units (AU) and the data are represented as mean ± standard error of mean (SEM).

The recovery of pADPr in IP extracts was also determined at the same time-points following MNNG exposure. Aliquots of IP extracts were hand-spotted on Amersham Hybond-N+ positively charged nylon membrane (GE Healthcare) and probed with anti-pADPr antibody clone 96-10. Dihydroxyboronyl Bio-Rex (DHBB) purified pADPr was used as a reference for the establishment of a standard curve for quantitation (24).

Immunoblotting

Whole cell extracts and immunoprecipitates were separated on 4–12% Criterion XT™ Bis–Tris gradient gel (Bio-Rad) and transferred onto 0.45 μm pore size PVDF membrane (Millipore). After a 1-h incubation with a PBS–MT blocking solution (PBS containing 5% non-fat dried milk and 0.1% Tween20), the membrane was probed overnight with primary antibodies (refer to Supplementary Methods for detailed information). Membranes were washed with PBS-MT and species-specific horseradish peroxidase-conjugated secondary antibodies were added for 30 min. Signals were detected with Western Lightning™ Chemiluminescence Reagent Plus kit (Perkin Elmer). Semi-quantitative data was obtained from the scanned films by drawing region of interest (ROIs) around the bands to be quantified. Background signal was subtracted from all images. Signal intensity was expressed as ratios based on density units from control samples using the GeneTool software (PerkinElmer). All data were represented as mean ± standard deviation (SD).

GeLC-MS/MS and label-free spectral counting

SDS–PAGE protein lanes corresponding to immunoprecipitates and negative non-specific IgG control extracts were cut into gel slices using a disposable lane picker (The Gel Company, CA, USA). In-gel protein digest was performed on a MassPrep™ liquid handling station (Waters, Mississauga, Canada) according to the manufacturer's specifications and using sequencing-grade modified trypsin (Promega, Madison, WI, USA). Peptide extracts were dried out using a SpeedVac and separated by online reversed-phase nanoscale capillary liquid chromatography (nanoLC) and analyzed by electrospray MS (ES MS/MS)

using a LTQ linear ion trap mass spectrometer (Thermo Electron, San Jose, CA, USA) equipped with a nanoelectrospray ion source (Thermo Electron, San Jose, CA, USA). All MS/MS spectra were analyzed using Mascot (Matrix Science, London, UK; version 2.2.0). Scaffold (version 03_00_02, Proteome Software Inc., Portland, OR, USA) was used to sum the spectral counts, validate MS/MS-based peptide and protein identifications and group peptides into proteins (refer to Supplementary Methods for detailed information).

Semi-quantified proteins by spectral counting analysis were grouped on the basis of their correlated time course profiles following treatment with MNNG. We first normalized every protein spectral counts independently by first subtracting the mean of the spectral counts and then dividing the result by the standard deviation (*Z*-scores). With this transformation, every protein has a mean of zero and 1 SD. Using the *fpc* package (25) in *R* statistical environment (http://www.r-project.org/), we then identified the optimal number of clusters by running the *pamk* function (25). Heatmaps corresponding to 5 min MNNG, 1 and 2 h clusters were generated using MeV software v4.6.1 (http://www.tm4.org/mev/). Functional classification and ID conversion of identified proteins were accomplished by using DAVID (http:/www.david.abcc.ncifcrf.gov).

Isobaric tag for relative and absolute quantitation

For isobaric tag for relative and absolute quantitation (iTRAQ) labeling, proteins were eluted from the Dynabeads with 6% SDS. Proteins were precipitated overnight with 4 volumes of acetone, centrifuged 15 min at 10 000*g* (4°C) and pellets were resuspended in 0.5 M triethyl ammonium bicarbonate (TEAB) containing 0.1% SDS. Samples were then reduced, alkylated, digested and labeled according to the standard protocol supplied by the manufacturer (Applied Biosystems iTRAQ™ Reagents—Chemistry Reference Guide, P/N 4351918A). iTRAQ results were generated from the analysis of four isobaric tags. Control was labeled with iTRAQ reagent 114. The MNNG samples of 5 min, 1 h and 2 h were, respectively, labeled with iTRAQ reagents 115, 116 and 117. Labeled peptides were lyophilized and resuspended in 630 µl of Milli-Q water. An aliquot (315 µl) of this solution containing 0.2% carrier ampholytes (Bio-Lyte 3/10, Bio-Rad) was used to rehydrate an 18-cm immobilized pH gradient gel strip (pH 3–6), and the other 315 µl containing 0.2% carrier ampholytes (Ready strip 7–10, Bio-Rad) was used to rehydrate a second 18-cm immobilized pH gradient gel strip (pH 7–10). Rehydratation was set for 10 h at room temperature without any voltage applied. Peptides were focused by applying a voltage of 250 V for 15 min, then 10 000 V for 3 h and finally 10 000 V for a total of 60 000 V•h. Immediately after focusing, each strip was cut into 36 segments of 5 mm for a total of 72 fractions. Gel pieces were transferred into a 96-well plate and peptides were eluted by first incubating the gel pieces for 15 min in 2% acetonitrile, 1% formic acid and then for 15 min in 50% acetonitrile, 1% formic acid. The extracted peptides were lyophilized using a SpeedVac and resuspended in 25 µl of 0.1% formic acid in water. An aliquot of 5 µl of this solution was used for LC-MS/MS analysis on an Agilent 1100 nanoLC system coupled to a QSTAR XL equipped with MDS nano ESI source. Raw data (wiff extension file) processing, protein identification, protein quantitation and statistical analyses were undertaken with ProteinPilot software v.3.0 (AB-Sciex) running the Paragon algorithm (25) (refer to Supplementary Methods for detailed information).

Stable isotope labeling by amino acids in cell culture

Incorporation of stable isotopically labeled amino acids in cell culture (SILAC) was performed essentially as described in (26,27). Briefly, HEK 293 cells were cultured in DMEM depleted of arginine and lysine. The DMEM was supplemented with 10% dialyzed FBS (Invitrogen, Carlsbad, CA, USA). Penicillin (100 U/ml) and streptomycin (100 mg/ml) (Wisent, Canada) were added to culture media with Arg and Lys containing naturally-occurring atoms (referred as the light culture) or their stable isotope counterparts [$^{13}C_6$ Lys and $^{13}C_6{}^{15}N_4$ Arg (Cambridge Isotope Labs, UK), referred to as the heavy culture]. Cells were grown for at least five divisions to allow full incorporation of labeled amino acids. Cells were tested for complete incorporation of the label. A bicinchoninic acid (BCA) protein assay (Pierce, Canada) was performed on each cell extract before the IP experiment to adjust equivalent amounts of starting material for each condition. The pADPr-associated protein complexes were immunoprecipitated and elulates were subjected to SDS–PAGE. The fractions were analyzed on a LTQ-Orbitrap Velos coupled to an Agilent 1100 Series nanoflow HPLC instruments using nanospray ionization sources. Protein identification and quantitation were done using Proteome Discoverer (v.1.2, ThermoFisher, Bremen, Germany) and Mascot (v.2.3, Matrix Science) to search against the human IPI database (refer to Supplementary Methods for detailed information).

Data-dependent bioinformatics

Gene ontology enrichment analysis

Gene Ontology (GO) term enrichment was performed using DAVID bioinformatics resources (http://david.niaid.nih.gov) (28) to determine whether particular GO terms occur more frequently than expected by chance in a given dataset. Default settings for the Biological Process category were used. The Cytoscape (29) plugin BiNGO (30) was also used to assess enrichment of GO terms and to generate diagrams.

Network construction and visualization

The Cytoscape plugins Michigan Molecular Interactions (MiMI) plugin (31) and BisoGenet (32) that both integrates data from multiple well known protein interaction databases were used to retrieve molecular interactions and interaction attributes. Direct protein interactions were displayed using Cytoscape (v2.7.0) using the corresponding official gene symbols. A subnetwork containing the

physical interactions between proteins involved in the DNA damage response was extracted from the main network (refer to Supplementary Methods for detailed information).

Recruitment of DNA damage response factors to laser-induced DNA damage sites

The recruitment kinetics of DNA damage response factors was assessed essentially as described (33) with the following modifications. After overnight transfections with Effectene reagent (Qiagen), HEK 293 cells expressing GFP fusion proteins were incubated with fresh medium containing 1 μg/ml of Hoechst 33342 for 30 min at 37°C. To study the pADPr-dependent recruitment of proteins at DNA damage sites, cells were incubated with 5 μM of PARP inhibitor ABT-888 for 2 h prior to micro irradiation and recruitment analysis. A 37°C pre-heated stage with 5% CO_2 perfusion was used for the time-lapse on a Zeiss LSM-510 META NLO laser-scanning confocal microscope (40X objective). Localized DNA damage was generated along a defined region across the nucleus of a single living cell by using a bi-photonic excitation of the Hoechst 33342 dye, generated with a near-infrared 750-nm titanium:sapphire laser line (Chameleon Ultra, Coherent Inc.) The laser output was set to 3% with 10 iterations, except for PARP-1 and XRCC1 which were adjusted to 2% to avoid signal saturation. A Multi-Time macro developed in-house for AIM software v3.2 (Zeiss) was used for image acquisition. Background and photobleaching corrections were applied to each datasets as described (34). A minimum of eight recruitments per construct were collected and analyzed. Mean recruitment curves were plotted with Kaleidagraph v4.03.

RESULTS

Isolation of pADPr-containing protein complexes

Before focusing on pADPr dynamics, we first conducted a large-scale proteome analysis using nanocapillary liquid chromatography-tandem MS (GeLC-MS/MS) to explore the protein composition of pADPr-associated protein complexes at the peak of pADPr accumulation in cells following MNNG exposure (MNNG 5 min). To validate and generalize our findings in HEK 293 cell extracts, pADPr IPs were additionally performed in HeLa whole cell extracts under the same experimental conditions. A schematic workflow of the study is illustrated in Figure 1. High-throughput protein–pADPr interactions have remained largely inaccessible owing to the transient nature of poly(ADP-ribosyl)ation. In a previous study (11), we reported that mouse monoclonal antibodies against pADPr, such as clone 10H, can efficiently pull down pADPr in poly(ADP-ribose) glycohydrolase (PARG) knocked-down cells. For the present study, we empirically optimized a low-salt lysis strategy that is both effective in extracting pADPr-binding proteins while preserving non-covalent interactions. Using slightly alkaline pH, low ionic strength, a zwitterionic detergent (CHAPS) and a potent PARG inhibitor, we were able to extract and preserve high amounts of pADPr over time.

A limitation associated with the use of 10H antibody is the low affinity for short pADPr molecules (less than 20 ADP-ribose residues) (35). However, long and complex (branched) polymers, which are formed following DNA damage induction, are well recognized by 10H antibodies. A complementary tool for the isolation of pADPr-containing complexes was also developed based on the use of a catalytically inactive GFP-PARG (PARG-DEAD) isoform. PARG shares structural similarity to the conserved and widespread family of ADP-ribose-binding macrodomain modules (15,36). In this view, our second approach can be considered as an affinity-purification technique similar to IP, except that a catalytically inactive macrodomain-like containing bait was used to pull down proteins trapped into pADPr-containing complexes. A macrodomain pADPr affinity resin, which consists of purified GST-Af1521 macrodomain (37) fusion protein bound to glutathione beads, was also used as a bait to capture pADPr-associated protein complexes. Addressing pADPr binding requires a systematic approach that can benefit from various alternatives.

Globally, we report the high-confidence identification of 609 proteins (33 621 MS/MS spectra, 2.7% peptide false discovery rate; a minimum of two unique peptides, Supplementary Table S1), which several of these are actually associated with the regulation of DNA repair and chromatin remodeling. The 10H and PARG-DEAD datasets share striking similarities but also express differences as PARG-DEAD datasets also include specific PARG-interacting proteins in addition to pADPr-associated proteins (Figure 2A). One important difference between the pADPr-associated protein datasets coming from antibody (10H) and PARG-DEAD approaches is the bias toward different cellular compartments. When a PARG-DEAD mutant is used as a substrate trapping bait to co-purify pADPr-binding proteins, the protein dataset is significantly enriched in nuclear proteins, whereas an antibody-mediated approach targets more mitochondrial proteins (Figure 2B). The vast majority of proteins identified with the Af1521 macroprotein pADPr affinity resin were also identified with the PARG-DEAD dataset, an observation consistent with the fact that PARG and Af1521 are both members of the ADP-ribose-binding macrodomain family. The macrodomain pADPr affinity resin protein dataset is exclusively composed of nuclear proteins that are coherent with its functions in nucleosome stability and regulation. Globally, a PARG-DEAD ligand binds a wider range of proteins and thus, represents a valuable tool for the isolation of pADPr-containing complexes. Furthermore, in this approach, the bait is expressed *in vivo* in mammalian cells, a feature that more accurately reflects physiological conditions.

Figure 2C graphically represents the peptide coverage of all the proteins identified at the peak of pADPr accumulation. Proteins are plotted according to the number of unique peptides assigned to each proteins (Supplementary Table S1). There is a correlation between protein abundance and the number of unique peptides identified for that protein. Generally, proteins anticipated as being in high abundance, such as PARP-1 in pADPr IP extracts,

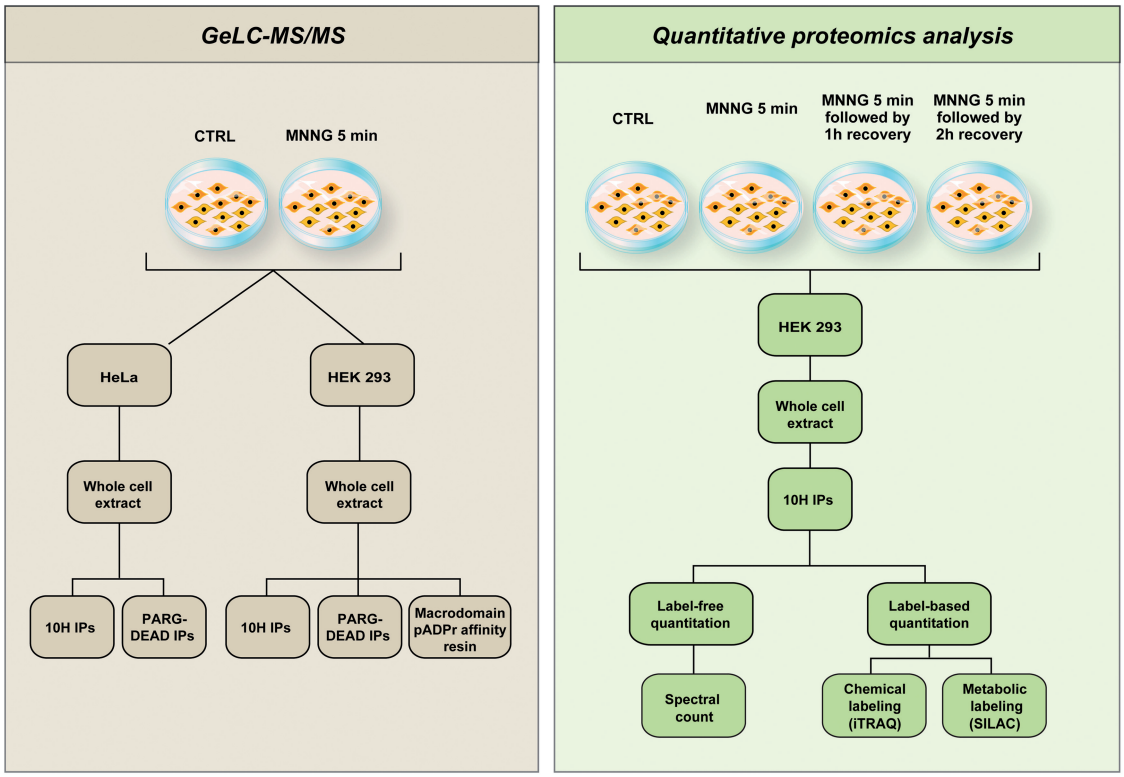

Figure 1. Schematic representation of the experimental design and proteomics strategies to identify pADPr-associated protein complexes. A combination of affinity-purification procedures coupled with MS was used to generate a global protein profile of pADPr-associated protein complexes (GeLC-MS/MS—left panel). Proteomics strategies that integrate relative quantitation with affinity-purification MS were used to provide a time-resolved proteome profile of protein networks responsive to pADPr turnover (right panel). Complementary label-free and label-based quantitative proteomics approaches were used to identify and evaluate protein changes occurring in cells following alkylation-induced DNA damage and PARP activation. 10H IPs: Immunoprecipitations with anti-pADPr antibody clone 10H; PARG-DEAD IPs: IP of catalytically inactive PARG, as described in the text.

are typically identified by the largest number of unique peptides. Proteins assigned with the fewest number of unique peptides are of low abundance. The fact that several DNA damage response (DDR) regulators scored prominently in either 10H-, PARG-DEAD- and macrodomain-based protein datasets support the biological relevance of both our overall screening strategy and the identification of additional top-scoring hits. Although a peptide count approach is not inherently quantitative, it provides rough estimates of protein abundance that are, in our experience, estimated fairly accurately as most of the pADPr-binding proteins known so far are among the proteins with the best peptide coverage. Selected nucleic acids binding proteins are displayed according to their estimated relative abundance (Figure 2C). In addition to PARP-1, the GeLC-MS/MS dataset also contains other PARP family members (PARP-2, PARP-9, PARP-12 and PARP-13) and numerous proteins involved in the maintenance of genome integrity. Most of the pADPr-binding proteins previously reported in other studies were identified using our affinity-purification procedures, including XRCC1 (9), LIG3 (9), KU70 (9), DNA-PK (9), CHD4 (38), CHD1L (ALC1) (39,40), DEK (41), NUMA (42), MVP (43), BUB3 (44), DNA-PK (45), DNMT1 (46), SUPT16H (47), TOP1 (48), TOP2B (49), hnRNPs (50,51) and histones (52).

High-quality spectra were also used to establish a list of proteins identified with unique peptides. Protein identifications were accepted if the corresponding peptide was assigned in at least two independent experiments (Supplementary Table S1). Examples include the chromodomain-helicase-DNA-binding protein 1 (CHD1), DNA repair protein RAD50 and the mitochondrial apoptosis-inducing factor (AIF) (53). The presence of RAD50, a component of the MRE11-RAD50-NBS1 (MRN) complex, was validated by western blot analysis in pADPr IP extracts (Figure 4A), an indication of the data quality.

Being confident that our pADPr isolation method is worthy and effective for the analysis of a wide range of pADPr-associated protein complexes, we further examined the time-dependent accumulation of DNA repair factors in pADPr pull-down extracts up to 2 h following genotoxic insult.

Time-resolved quantitative proteomics analysis of pADPr-containing protein complexes

The insights gained by the identification of pADPr-associated protein complexes and their DNA damage response pathways can provide valuable clues pointing to target proteins. A major challenge is to understand the

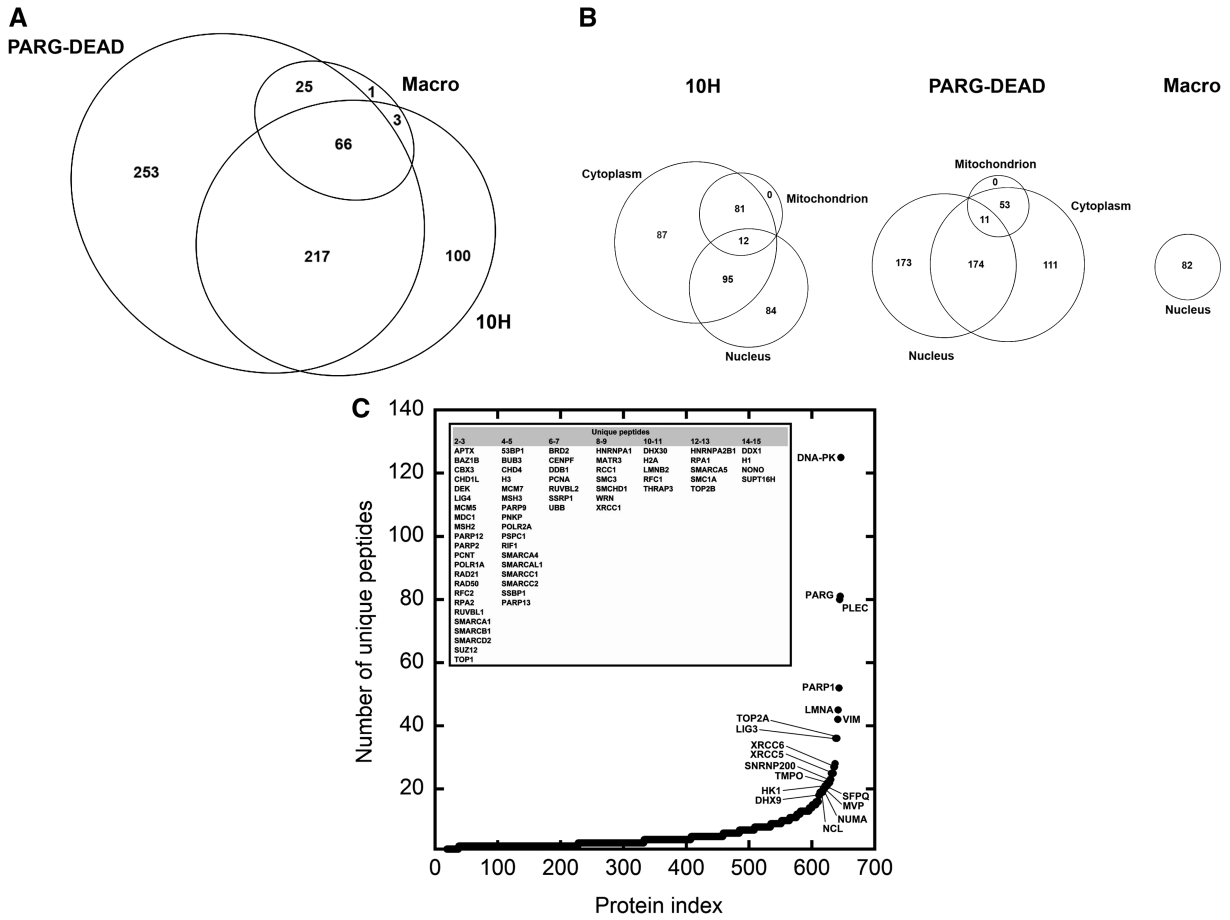

Figure 2. Diversity of pADPr-associated proteins as revealed by gel-based LC-MS/MS analysis. Complementary proteomic approaches directed towards identification of novel proteins that interact with pADPr were integrated to mine the accessible pADPr-binding interactome. IPs were performed directly against pADPr using a high affinity monoclonal antibody (clone 10H) or indirectly by a novel pADPr substrate trapping approach targeting a catalytically inactive PARG mutant and a macrodomain protein (see text for details). (**A**) The area-proportional Venn diagram shows unique and shared protein identifications in pADPr-associated protein datasets that originate from each strategies. (**B**) Area-proportional Venn diagrams depicting the distribution of proteins in subcellular compartments for each datasets. Proteins were classified into cytoplasmic, nuclear or mitochondrial compartments according to GO classification. (**C**) Classification of pADPr-associated proteins. Proteins are ordered relative to the number of unique peptides assigned. The inner frame lists some DNA damage response factors and chromatin-associated proteins with their corresponding number of unique peptide assignments. Refer to Supplementary Table S1 for detailed protein listing.

dynamic behavior of these targets with respect to pADPr. This requires knowledge of the protein dynamics in complex molecular signaling systems tethered together via interactions with heterogeneous pADPr. A mean of generating quantitative information on protein networks responsive to DNA damage is to investigate which network components of these are actually accumulating in affinity pull-down experiments targeting pADPr.

Western blot analysis of DNA damage recognition and repair factors in pADPr IP extracts at sequential time-points following PARP activation

To make further analysis on the pADPr-associated interactome, we examined the dynamic changes of the pADPr-associated protein complexes composition by time course analysis of pADPr proteome changes following exposure to MNNG-induced DNA damage. This approach needed to conciliate two opposite requirements. Since the half-life of pADPr in cells is estimated to be <1 min, pADPr hydrolysis must be limited in order to preserve pADPr pools with respect to the time required by the pull-down assay. On the other hand, a complete disruption of pADPr turnover is not desirable since it would block the dynamics of the targeted protein complexes. To overcome this challenge, the use of a competitive PARG inhibitor (ADP-HPD) (54) appeared to be very appropriate. In contrast to an RNAi-based specific knock-down of PARG resulting in sustained cellular pADPr levels for a prolonged period of time (11), the use of a PARG inhibitor in cell extracts at the time of lysis enables the normal modulation of cellular pADPr levels, whereas stabilizing pADPr in cell extracts required for efficient pull-down assays. The turnover of pADPr was estimated by polymer-blot analysis and immunofluorescence. Hand-spotted DHBB-purified pADPr (24) was used as reference to estimate pADPr content in IP extracts (Figure 3A). We were able to recover more than 10 pmol of pADPr/10^6 cells, which represent a significant fraction of total pADPr formed during alkylation-induced DNA damage (55,56). Immunostained

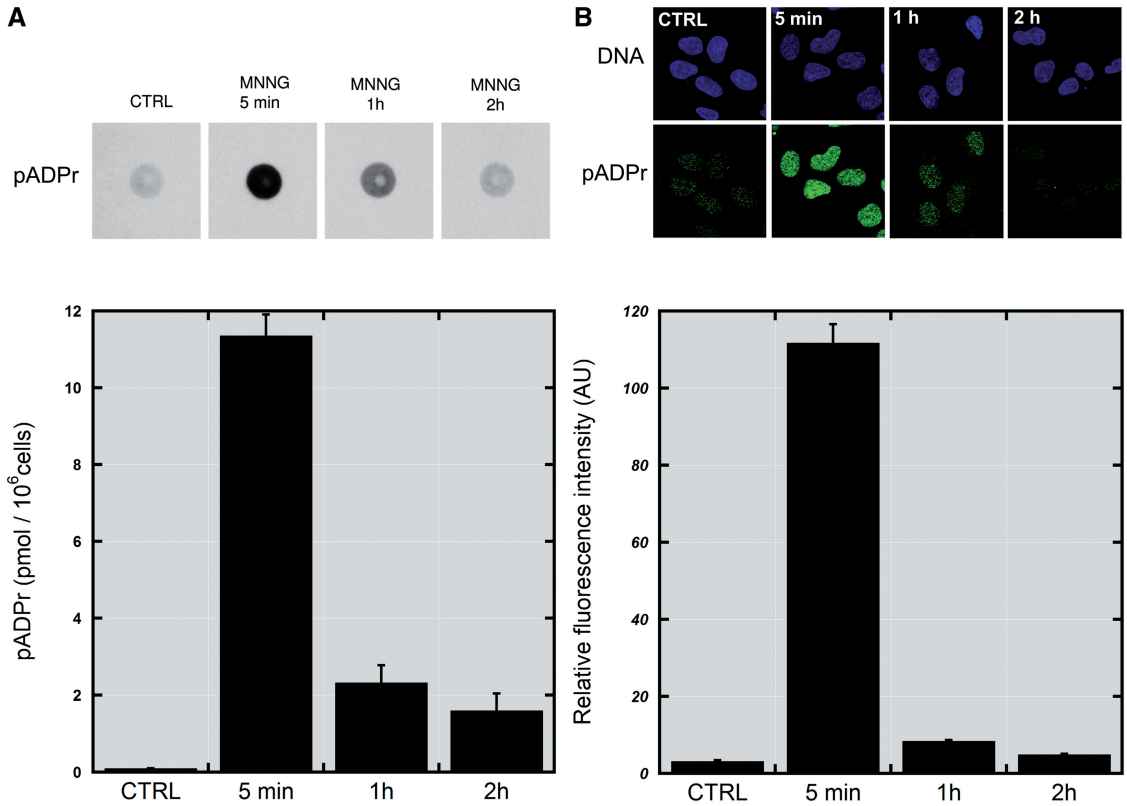

Figure 3. pADPr dynamics following MNNG-induced DNA damage and PARP activation. (**A**) Dot-blot analysis of pADPr levels in pADPr IP extracts from MNNG-treated HEK 293 cells. Cellular material bound to 10H-coupled magnetic beads was eluted and hand-blotted on positively charged nylon membrane. pADPr was detected using 96-10 antibody (upper panel). pADPr signals in IP extracts were quantified using DHBB-purified pADPr as a reference value for quantitation and displayed on a bar graph (lower panel). The data are represented as the mean ± SEM ($n = 4$). (**B**) The 10H immunofluorescence labeling of pADPr in HEK 293 cells exposed to MNNG (upper panel). Confocal fluorescent images were obtained by a Zeiss LSM 510 NLO laser scanning confocal microscope. A region was drawn inside of each nucleus ($n = 100$) to establish the mean fluorescence intensity. Relative pADPr levels were plotted on a bar graph (lower panel) and displayed as the mean ± SEM ($n = 3$).

pADPr quantitation indicate that the recovery of pADPr by IP closely match the turnover of pADPr in living cells (Figure 3B). Cellular pADPr levels reach a maximum (30- to 50-fold increase) after 5 min of MNNG treatment and subsequently decrease to basal levels. After a 2-h recovery period, pADPr is nearly undetectable by western blot except for PARP-1, which remains significantly automodified (Figure 4A). In contrast, pADPr shows a wide distribution at peak levels from the loading well down to the low molecular weights at the bottom of the blot. This ADP-ribose polymers' size distribution of the products generated by PARPs and PARG interplay are presumably the consequence of the resolution of free and protein-bound pADPr from various lengths and branching frequencies. We therefore hypothesized that pADPr-containing DNA repair complexes would primarily be isolated in this fraction. As expected, several DNA repair factors are trapped in immunoprecipitates corresponding to MNNG-treated cells, with a predominant enrichment in the 5 min sample that contains the highest levels of pADPr (Figure 4A). The presence of PARP-1 and its high-confidence interactors indicates that pADPr-associated protein complexes are efficiently pulled down. The relatively high level of PARG present in these samples also validates the presence of poly(ADP-ribose) degrading enzymes in these fractions.

Semi-quantitative analyses of protein levels were measured by densitometry scanning of western blots shown in Figure 4A. Profiles were generated for every targeted DNA damage response (DDR) factors and their abundance was correlated to pADPr dynamics (Figure 4B). The base excision repair (BER) pathway clearly shows a prominent association with pADPr, especially as core components of the BER pathway (LIG3 and XRCC1) are hard to detect in control conditions that correspond to the pull down of pADPr-containing complexes in the absence of genotoxic insult. This result is consistent with the preferential interaction of the XRCC1/LIG3 complex with the poly(ADP-ribosyl)ated form of PARP-1 (57). In contrast, components of the non-homologous end joining (NHEJ) and HR repair pathways are more stably associated with pADPr-containing complexes under basal conditions, a characteristic that tends to temper the relative accumulation ratios after DNA damage.

As a proof of concept, we identified several DDR targets by western blot analysis of anti-pADPr immunoprecipitates with a global accumulation trend that

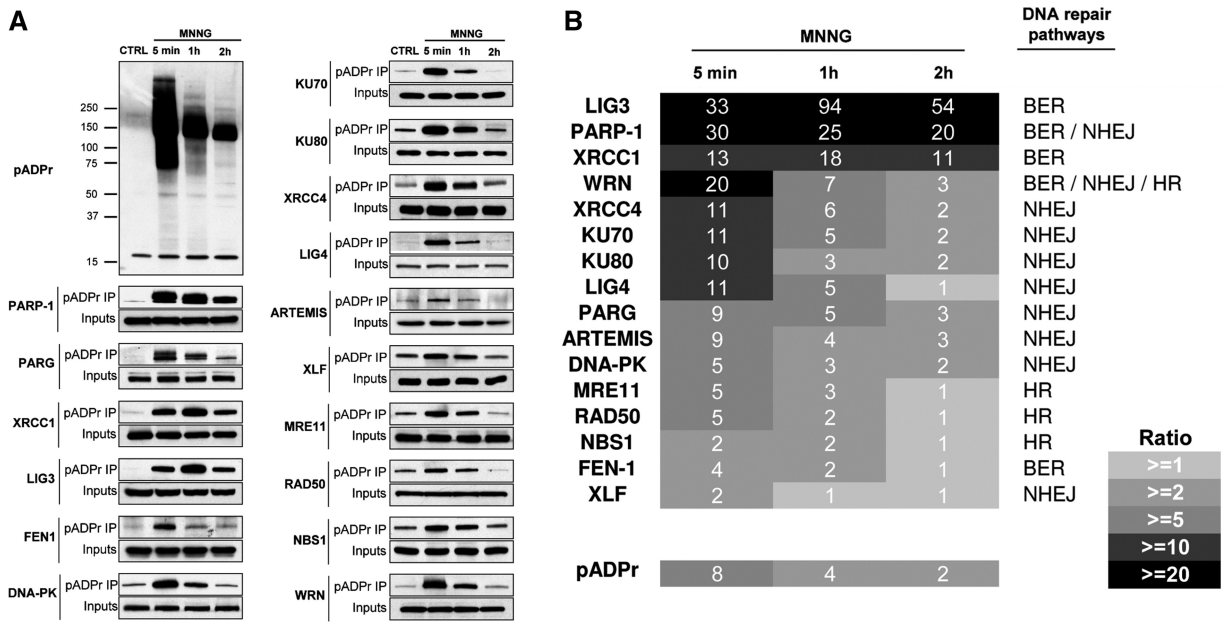

Figure 4. Correlated accumulation of DNA damage response factors with pADPr. (**A**) The 10H-based IPs using HEK 293 whole cell extracts were performed to isolate pADPr-associated proteins in the context of MNNG-induced DNA damage and PARP activation. Cells were allowed to recover from MNNG by incubation with fresh medium and IPs were performed at the indicated times. Undamaged control cells were pre-incubated 2 h with 5-μM PARP-1 inhibitor ABT-888 before lysis. Several DNA damage response factors were screened for entrapment in anti-pADPr IP extracts. Cell lysates (inputs) were also subjected to western blot analysis using the corresponding antibodies. (**B**) pADPr levels correlate with the accumulation of several DNA damage response factors involved in major DNA repair pathways. Relative quantitation of western blot signal intensities shown in (A) were measured and expressed relative to control protein levels. A greyscale heatmap ranks each of the protein accumulation ratios.

correlates to pADPr levels. This observation led us to further explore the dynamics of pADPr-associated complexes by quantitative MS.

Quantitative proteomics analysis of complex protein mixtures in pADPr IP extracts

Quantitative proteomics can reveal changes in protein abundance that can be indicative of a component that has affinity for pADPr or likely part of pADPr-modulated protein complex, including previously undescribed factors. Several relative and absolute quantitative proteomics techniques have been developed in recent years. Generally, MS-based quantitation methods fall into two categories: label-free or label-based approaches (58), each having specific strengths and limitations (59). Whereas most quantitative proteomics studies rely on either strategy, we undertook a more systematic approach for a thorough analysis of the pADPr proteome (Figure 1).

Label-free quantitation

The spectral counting method has become an accepted technique to estimate the relative abundance of proteins in highly complex samples. Spectral counting is a large-scale strategy easily applicable to GeLC-MS/MS protein identification. One of the main advantages of the method is that it does not require the use of high resolution mass spectrometers such as those required for quantitative label-based MS approaches.

Antibody-mediated affinity purification of pADPr-containing protein complexes was performed in HEK 293 whole cell extracts after exposure and release from MNNG-induced DNA damage and PARP activation. Untreated cultures were used as a basis for calculating protein ratios derived from peptide spectral counts. A set of 425 proteins was identified (Supplementary Table S2) from which we extracted 275 proteins that follow a kinetics pattern that clusters them into one of the three time-points analyzed after MNNG exposure (Figure 5A). *K*-means clustering is one of the most popular partitioning method. We used a robust version of *K*-means clustering based on medoids by using the *pamk* function (partitioning around medoids) (25) to group proteins identified during our screen based on their time course profiles following exposure to MNNG. The goal of the algorithm is to segregate each protein dynamics into the profiles that they most closely matched. Partitioning around medoids is more robust than *K*-means in the presence of noise and outliers, an interesting feature since pADPr-associated proteins exhibited significant variability over a wide range of ratios. By clustering proteins with similar accumulation trend, we were able to obtain a clear snapshot of protein enrichment in relation with pADPr dynamics (Figure 5A). We hypothesized that proteins with a distribution pattern that correlates with pADPr levels are presumably proteins with close connection with pADPr, whether by being covalently poly(ADP-ribosyl)ated, non-covalent pADPr-binders or major components of pADPr-associated protein complexes.

The top biological processes associated with each clusters of proteins were identified using DAVID bioinformatics resources (Functional gene classification tool based

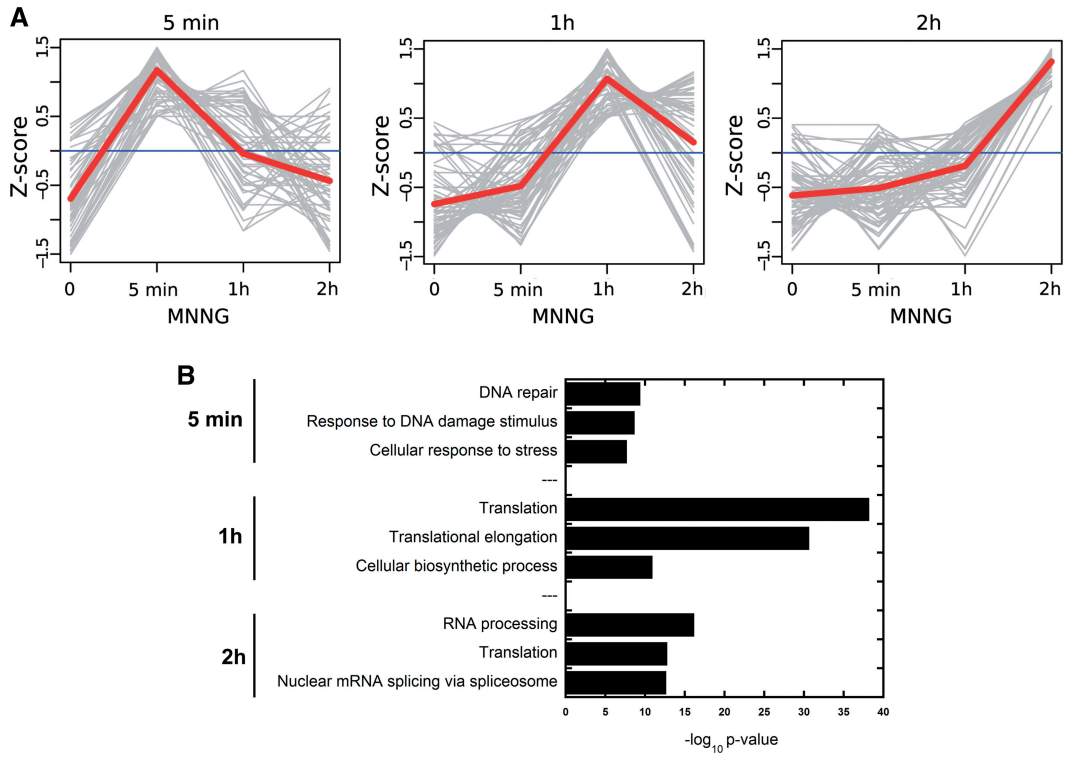

Figure 5. Protein abundance profiles in time-resolved pADPr IPs. Spectral counting-based quantitation was combined with Scaffold's protein validation tools to provide a quantitative protein profile. pADPr-associated proteins identified by GeLC-MS/MS in IP extracts were grouped by *K*-means clustering for each treatment, respectively. (**A**) The kinetics of protein accumulation is displayed by trend curves showing the overlay of the proteins grouped by each cluster. The red line represents the mean value at each time-point for all the proteins in the cluster. (**B**) Protein clusters were searched for significant over-representation of proteins belonging to specific pathways according to the GO database using DAVID. Bar plots of the most significant biological processes in each datasets are shown. The significance of the enrichment is expressed as a function of the *P*-value, which indicates whether a biological process is significantly higher than random expectations. Refer to Supplementary Table S2 for complete protein listing.

on GO terms)(28). Biological processes were displayed as *P*-value bar plots (Figure 5B). The *P*-values represent the probability to see a random enrichment in the displayed biological process. As cells recover from genotoxic stress, we can observe an evolution of the major biological processes associated with pADPr turnover. Although there is an overlap among the processes, the first predominant biological process identified at the peak of pADPr levels (MNNG 5 min) is related to DNA damage response which is consistent to the rapid activation of PARPs and pADPr synthesis in response to DNA strand breaks. After a 1-h recovery period from MNNG exposure, proteins involved in translationnal processes are highly over-representative of the pADPr-associated proteome, whereas regulatory circuits that control mRNA splicing, stabilization and translation are most prominent after 2 h. Individual protein accumulation trend was displayed in a heatmap for the three time-points analyzed after MNNG exposure (Figure 6). Proteins were grouped according to their kinetics profile. As we could expect, one can observe that PARP-1 is closely related to the kinetics of XRCC1 and LIG3, two stably associated components of the BER pathway. Similarly, KU80 (XRCC5), DNA-PK (PRKDC) and the facilitator of chromatin transcription (FACT) complex subunit SSRP1 are grouped together soon after the induction of DNA damage in the 5-min MNNG cluster. This approach could help to better focus on pADPr-responsive protein complexes involved in biological processes that contain numerous components such as those observed at later time-points following the induction of DNA damage.

Label-based quantitation: iTRAQ and SILAC analysis

SILAC (60) and iTRAQ (61) are two widely used methods to quantify protein abundance in tissue cultures. Whereas SILAC involves metabolic incorporation of isotope mass tags directly into proteins, iTRAQ chemical labeling is performed on peptides after lysis and trypsin digestion. Both SILAC and iTRAQ strategies were coupled to pADPr affinity-purification for the quantitation of protein abundance in time-resolved IP extracts following MNNG-induced DNA damage and PARP activation. Ratios of protein abundance were estimated based on datasets from untreated cells that correspond to basal levels of poly(ADP-ribosyl)ation in the absence of genotoxicity. As for any quantitative differential analysis, the most interesting identifications are those that differ by a substantial amount from the rest of the data (outliers). Box plots are particularly useful to display the distribution of a dataset and pinpoint those outliers. Figure 7 shows the box plot diagrams of iTRAQ and SILAC experiments. All the outlier values correspond to important protein accumulation in pADPr IP extracts. The intensities of the ratios and the number of outliers

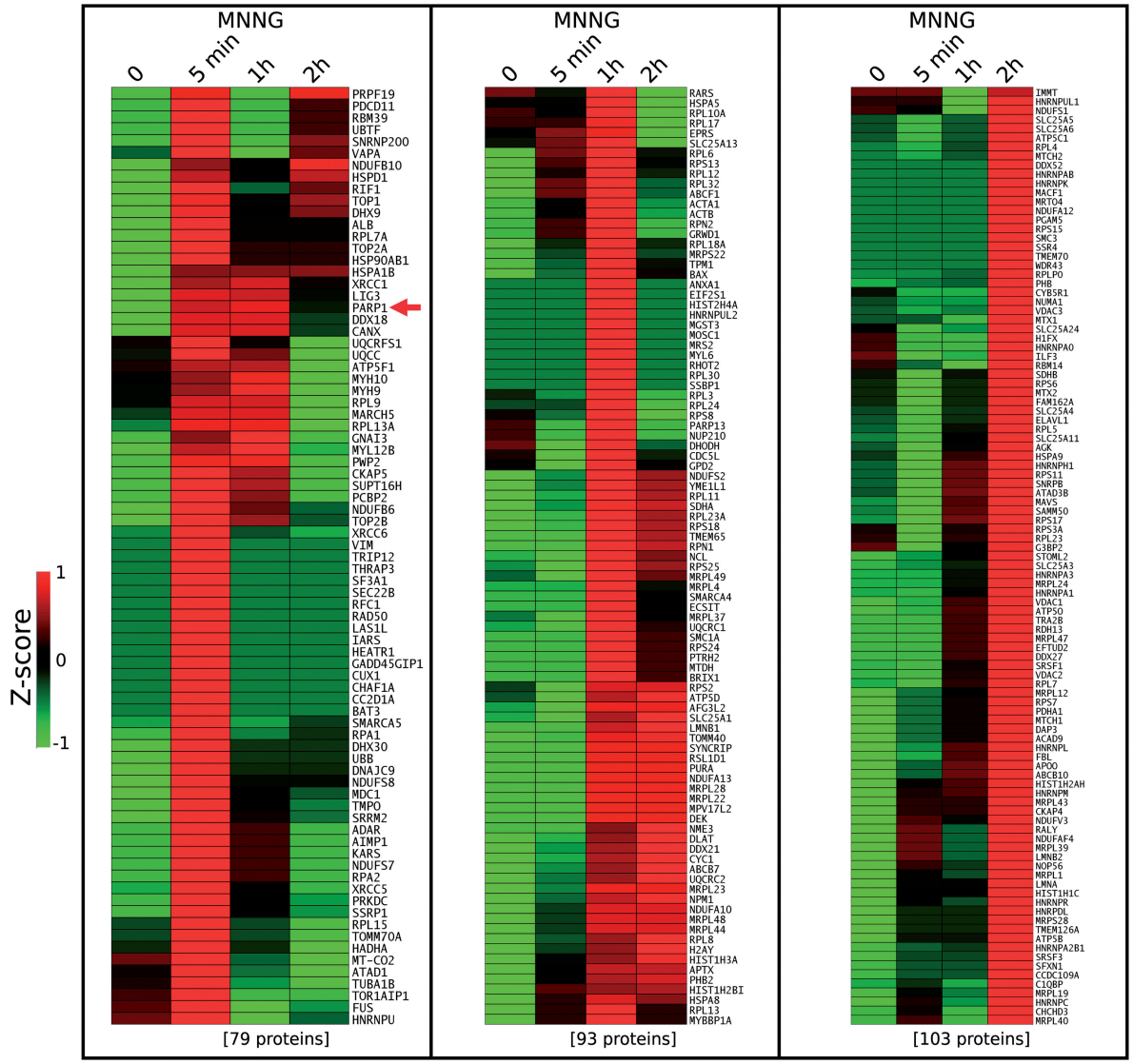

Figure 6. Heatmap analysis with *K*-means clustering. Temporal profiling of pADPr-associated proteins in HEK 293 cells upon MNNG exposure was performed based on the GeLC-MS/MS spectral count quantitation. The heatmap displays the three clusters identified by the *K*-means algorithm that correspond to the time-points analyzed after MNNG exposure. Green indicates the lowest ratio, black indicates an intermediate value and red indicates the highest ratio (protein enrichment). Proteins in each cluster are listed according to their gene symbol. A red arrow indicates the presence of PARP-1.

decrease as we proceed from 5 min to 1 h and 2 h post-MNNG treatment, an observation consistent with the progressive decrease of pADPr levels. Detailed iTRAQ and SILAC datasets are listed in Supplementary Table S3 and S4.

Although they are based on different approaches, iTRAQ and SILAC analysis reported a similar set of enriched proteins in pADPr IP extracts. The BER (XRCC1, LIG3) and the NHEJ (DNA-PK (PRKDC), XRCC5(KU80), XRCC6(KU70) multiprotein repair complexes are consistently found with both methods, as well as the facilitates chromatin transcription (FACT) complex subunits SSRP1 and SUPT16H. Proteins forming the nuclear lamina (LMNA, FLNA, TMPO) are also found with high ratios in consistency with their relative abundance found in GeLC-MS/MS dataset. Of particular interest are other factors that follow the same accumulation trend as did well characterized pADPr-binding proteins, suggesting a close link with poly(ADP-ribosyl)ation and chromatin functions. Proteins with high ratios such as barrier-to-autointegration factor (BANF1), single-stranded DNA-binding protein (SSBP1) or the thyroid hormone receptor-associated protein 3 (THRAP3) have not been characterized in the context of pADPr metabolism. However, PARP-1 has been found as a chromatin-associated partner of BANF1 (62); SSBP1 localizes in H2AX/PARP-1 complexes (63) and THRAP3 is a component of the human mediator complex that functionally interacts with PARP-1 (64).

Each label-based quantitation method had its own strengths. For example, only SILAC analysis identified APLF (Aprataxin and PNK-like factor) as one of the most enriched protein in 5-min MNNG

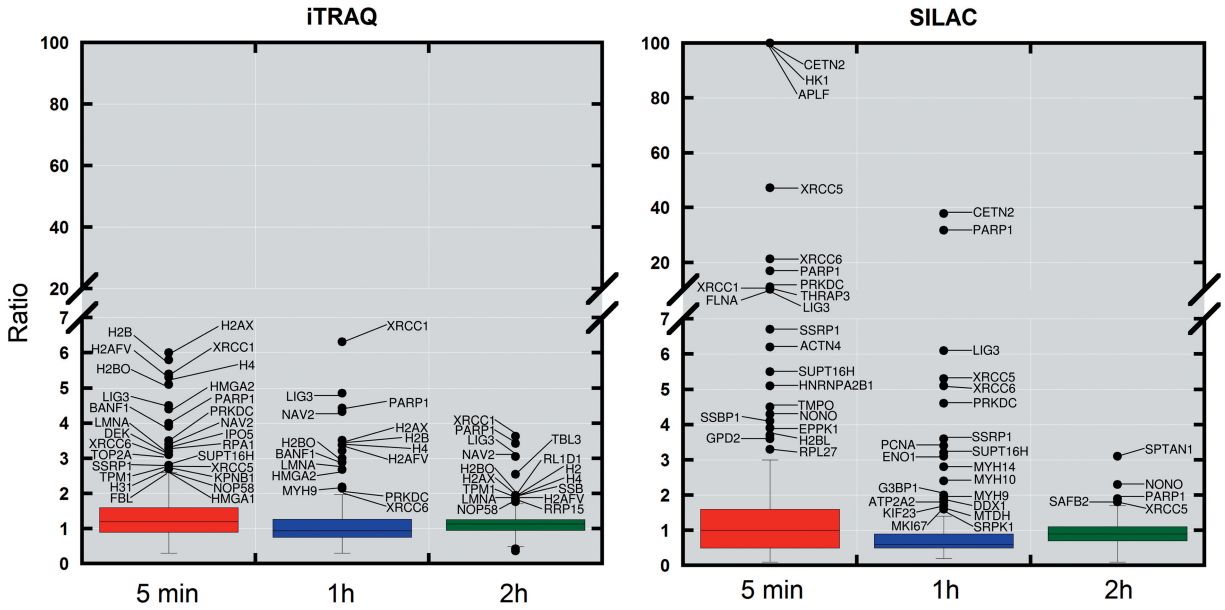

Figure 7. Box plot statistics to define outlier significance for iTRAQ and SILAC analysis. pADPr IPs were carried out after each of the three time-points examined following MNNG exposure. Protein isolates were quantified with respect to basal levels of pADPr in control IPs. Each box encloses 50% of the data with the median value of the variable displayed as a line. The top and bottom of the box mark the limits of upper and lower quartiles. The vertical lines extending from the top and bottom of each box mark the minimum and maximum values within the data set that fall within an acceptable range (1.5 × interquartile distance). Any value outside of this range (outlier) is displayed as an individual point with the corresponding gene symbol. Refer to Supplementary Table S3 (iTRAQ) and Supplementary Table S4 (SILAC) for detailed protein annotations.

immunoprecipitates. This is consistent with the fact that APLF contains a pADPr-binding PBZ motif (5,65,66). In addition to APLF, centrin-2 (CETN2) and hexokinase-1 (HK1) were identified with high ratios. However, in such cases, quantitations were based on unique peptides so the measured ratios must be tempered. Finally, one should keep in mind that the proteins displayed in iTRAQ and SILAC box plots (Figure 7) are those with extreme values with respect to the entire dataset. Proteins with more modest enrichment ratios that fall within the upper quartile (75th percentile) still represent interesting pADPr-associated candidates. For example, the stress granule-associated PARP-13 was identified in each of the time-points analyzed by SILAC but only after 2 h of MNNG exposure did it stand out from the protein dataset. Another example is NUMA, a poly(ADP-ribosyl)ated protein only found in the 2-h MNNG SILAC dataset with the same modest ratio as DNA-PK (PRKDC), SSBP1 and Mediator of DNA damage checkpoint protein 1 (MDC1) (Refer to Supplementary Tables S3 and S4 for detailed information).

Protein network modeling of pADPr-associated proteins

To gain insight into the dynamics of pADPr-associated proteins, we mapped a protein interaction network based on datasets derived from MS analysis. The global pADPr-responsive proteome modeled on the basis of all the proteins identified in this study resulted in a network of 959 proteins (nodes) and 8931 interactions (edges). The entire network is provided for interactive visualization of protein interactions in the Cytoscape session file (Supplementary Material). The network can be easily loaded and visualized using Cytoscape, which if freely available for download as an open source bioinformatics software (www.cytoscape.org). The ClusterOne algorithm was used to detect clusters of highly connected multiprotein complexes in the global network with associated confidence values. A group of 6 clusters with $P < 0.05$ were detected and extracted from the global pADPr proteome. These clusters includes (i) ribosomal proteins (93 proteins), (ii) polyubiquitin-C substrates (200 proteins), (iii) mitochondrial proteins (53 proteins), (iv) mRNA splicing and maturation factors (68 proteins), (v) components of the nuclear pore complex (24 proteins) and (vi) a small group of proteins involved in mitotic cell cycle (7 proteins) (Supplementary Cytoscape session file). To provide context and a more targeted view of our quantitative analysis of the pADPr-responsive proteome, we isolated a subnetwork of proteins that reflects significant molecular events linked to DNA damage response and pADPr metabolism. We extracted the first neighbors (direct protein–protein interactions) linked to protein components of the main DDR pathways found in our proteomics datasets. All the PARPs identified in this study were extracted in addition to components of the BER (XRCC1, LIG3), NHEJ (DNA-PK, XRCC5, XRCC6) and the FACT complex (SUPT16H, SSRP1). This subnetwork, composed of 164 nodes and 899 edges highlights the emerging importance of pADPr in the regulation of DDR (Figure 8). The most enriched proteins in pADPr IPs from GeLC-MS/MS, spectral counting, iTRAQ and SILAC datasets (top-scoring proteins) were flagged to underscore their relative abundance. The third quartile value was selected as the cut-off criteria (cut-off point for the highest 25% of the observed ratios;

Supplementary Table S5). This complex network structure represents a part of the DNA damage and repair response protein interaction map closely related to PARP-1 and highlights the value of integrating protein interaction information as it reveals potential pADPr-binding candidates to prioritize for functional follow-up. Interestingly, almost all the PARP-1 subnetwork (160 out of 164 proteins) connects to polyubiquitin-C (UBC) according to the interaction databases (Supplementary Cytoscape session file).

Dynamic recruitment of DNA damage response factors to sites of DNA damage

Whichever method was used to explore the pADPr interactome during alkylation-induced genotoxic stress, components of the BER and NHEJ repair pathways scored prominently in the quantitative protein profiles. The consistency of this observation strongly suggests that pADPr could be an important effector involved in the regulation of these repair processes. It had already been recognized that localized pADPr formation facilitates the accumulation of DNA repair factors at sites of broken DNA (67). This is particularly critical for the scaffolding protein XRCC1 for which recruitment at DNA damage sites depends on the presence of pADPr (68–70). In order to study the dynamic recruitment of DNA repair factors, we used a combination of Hoechst 33342 incorporation and near-infrared 750-nm two-photon laser micro-irradiation to induce DNA damage in subnuclear regions of single cells (Figure 9A). As expected, most of the DDR factors targeted in this study are recruited at laser-induced DNA damage sites (Figure 9B). The contribution of pADPr to the recruitment process of DNA repair factors was evaluated by treating the cells with

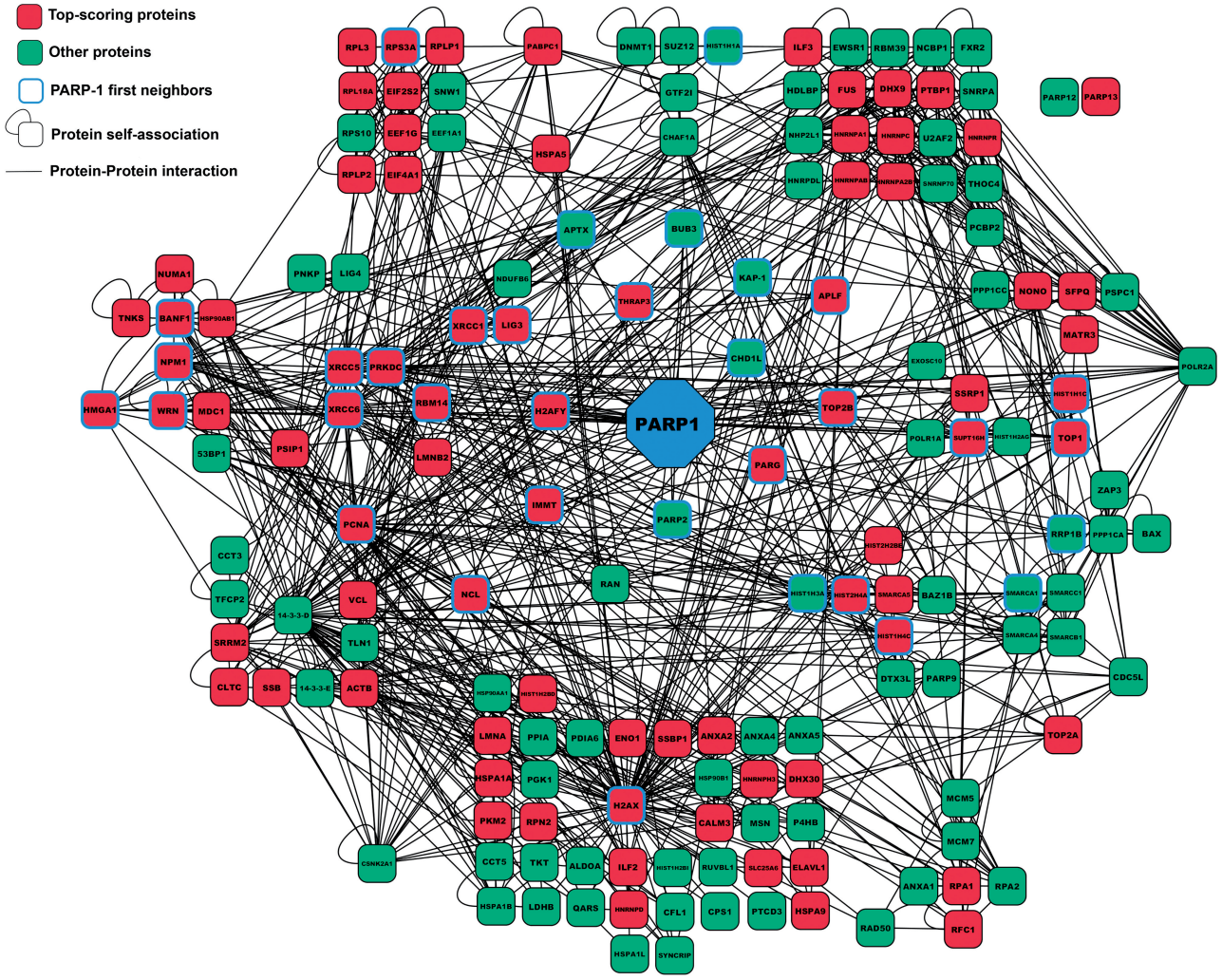

Figure 8. Subnetwork diagram of the PARP-1-centered protein interaction map. Cytoscape was used to construct a global network of the pADPr-associated proteome that integrates protein identification from all the proteomics approaches that have been carried out in this study. The diagram shown consists of the nearest-neighbors subnetwork of PARP family members in addition to selected proteins from DNA damage response pathways (See text for details). The subnetwork emphasizes the pADPr-associated protein regulatory network centered around PARP-1 in cellular recovery to DNA damage. The red coloring indicates top-scoring proteins and refers to predominant proteins in either of the four datasets (GeLC-MS/MS, Spectral count, iTRAQ, SILAC). Interactions among proteins are reported. The network comprises 164 proteins (nodes) and 899 interactions (edges). Refer to Supplementary Table S5 for complete protein listing.

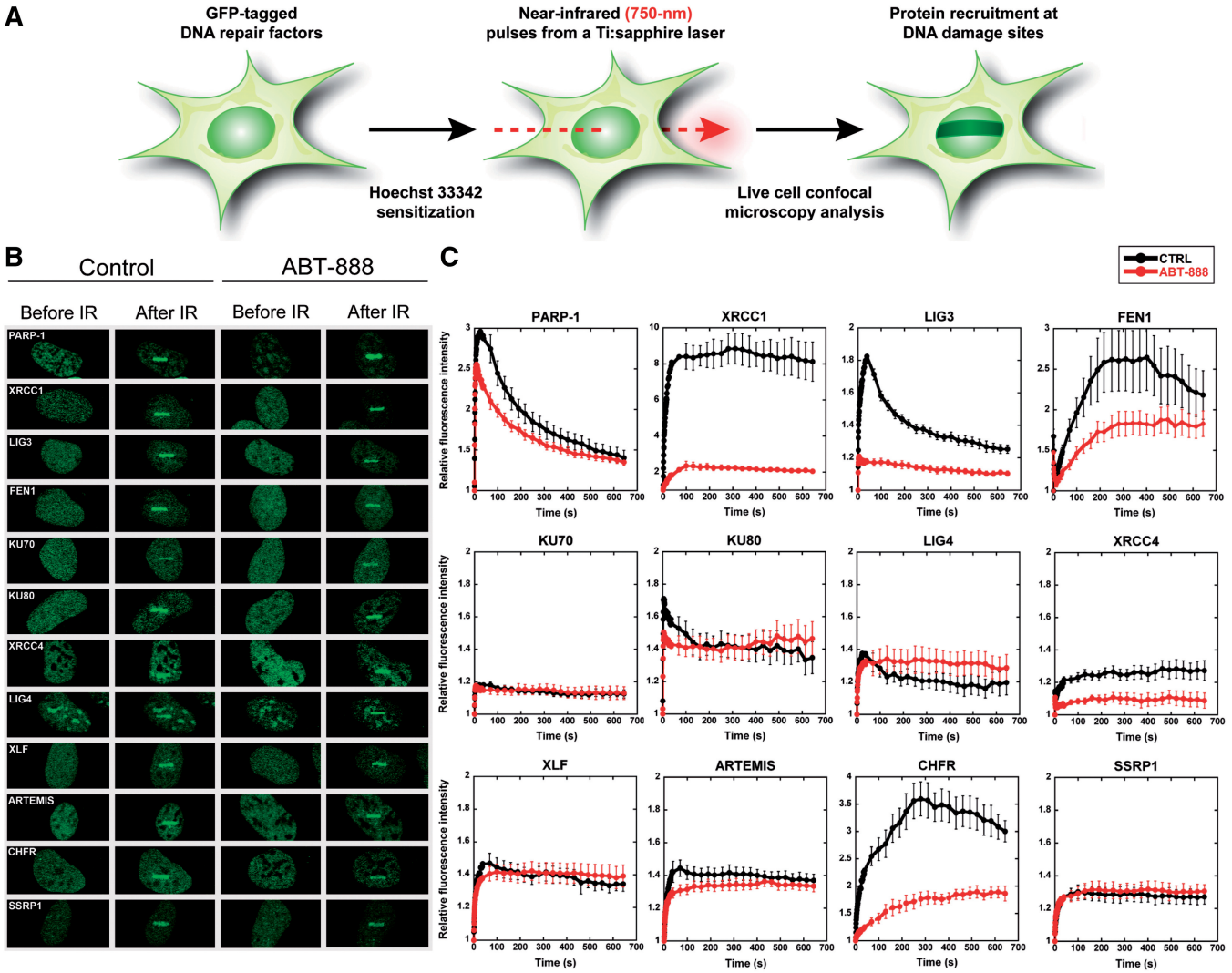

Figure 9. Dynamics of DNA damage response proteins at laser-induced DNA breaks. DNA damage induced by laser micro-irradiation in sub-nuclear region of single living cells was performed to evaluate the pADPr-dependent recruitment of DNA repair factors at DNA damage sites. (**A**) Schematic representation of the micro-irradiation system used to introduce DNA lesions. (**B**) Local accumulation of DNA repair factors at laser-induced DNA damage sites. A 750-nm two-photon laser beam was focused on Hoechst-sensitized cells and the accumulation of GFP-tagged DNA repair factors was monitored on a Zeiss LSM 510 NLO laser scanning confocal microscope. (**C**) Evaluation of the contribution of pADPr to the recruitment kinetics of DNA damage response factors at sites of DNA damage. The dynamics of several GFP-tagged proteins involved in DNA repair pathways were analyzed in the context of PARP inhibition (ABT-888). The HEK 293 cells transiently expressing the targeted proteins were sensitized with Hoechst 33342 and micro-irradiated with femtosecond near-infrared (750-nm) pulses from a Ti:sapphire laser. The intensity of fluorescence was recorded on a Zeiss LSM 510 NLO laser-scanning confocal microscope. The dynamics of DNA repair factors under normal conditions was compared with the dynamics observed following PARP inhibition with 5 μM ABT-888. Targeted proteins involved in BER (XRCC1, LIG3, FEN1), NHEJ (KU70, KU80, LIG4, XRCC4, XLF, ARTEMIS) and chromatin remodeling (CHFR, SSRP1) are displayed. Because of the rapid accumulation of DNA repair proteins at DNA damage sites, multiple acquisition rates were used (see 'Materials and Methods' section). Background and photobleaching corrections were applied to each dataset. A minimum of eight recruitments per construct were collected and analyzed. The error bars represent the SEM.

the potent PARP inhibitor ABT-888 [reviewed in Ref. (71)]. We first focused on XRCC1 to validate our approach since its pADPr-dependent accumulation at DNA damage sites was clearly demonstrated. Indeed, XRCC1 recruitment at DNA damage sites is severely decreased when PARP-1 is inhibited (Figure 9C). Because XRCC1 acts as a coordinator of BER, we anticipated that PARP-1 inhibition would lead to a reduced accumulation of LIG3 and other BER-associated factors. Although recruited at DNA damages sites with less intensity than XRCC1, we observed a decreased relocation of LIG3 when PARP activity is inhibited. A similar dynamics was observed for the Flap endonuclease 1 (FEN1) which also possesses functions in the BER system. These results underscore the role of pADPr in facilitating the recruitment of BER factors and are consistent with the identification of these factors as some of the most enriched proteins in pADPr IP extracts.

Following the same idea, we anticipated that the recruitment of major components of the NHEJ repair pathway

at DNA damage sites would also be influenced by a decrease in the accumulation of pADPr. We did see a modest recruitment of each of the targeted NHEJ factors in the path of the laser track (KU70, KU80, XRCC4, LIG4, XLF and ARTEMIS) but none of these showed a significant dependence on pADPr to localize at DNA damage sites (Figure 9C).

In addition to DNA repair events, extensive chromatin remodeling and histone modifications occur at sites of DNA damage. Following this idea, our attention was directed toward a chromatin remodeling complex consistently trapped in pADPr IP extracts, namely the FACT complex SUPT16H/SSRP1 that acts to reorganize nucleosomes. As a control, we used CHFR, a chromatin remodeling protein that regulates histone modifications and the ATM-dependent DNA damage response pathway after DSBs (72). CHFR possesses a PBZ domain known for its non-covalent interaction with pADPr. As expected, CHFR recruitment and retention at DNA damage sites is strongly decreased in presence of ABT-888, whereas SSRP1 recruitment is unaffected (Figure 9C). In our protein clustering experiment, we found that SSRP1 accumulation profile with respect to pADPr closely match those found for KU80 and DNA-PK (Figure 6, 5-min MNNG cluster). SSRP1 was also found with high ratio in iTRAQ and SILAC experiments (Figure 7) along with its stable partner SUPT16H. The modest intensity of SSRP1 accumulation at DNA damage sites falls within a similar range as that for the NHEJ factors and this accumulation is also pADPr-independent.

DISCUSSION

This study represents the first reported proteome-wide effort to follow protein dynamics in the context of pADPr modulation after DNA damage. In addition to the exploration of the pADPr-associated proteome with antibody-mediated affinity purification, MS-based substrate trapping strategies were used as complementary approaches to mine the accessible pADPr-associated proteome. These analyses suggest that the presence of pADPr in many multiprotein complexes involved in genome surveillance could be functionally relevant. Yet, these complexes are not static, but instead are dynamic assemblies that orchestrate DNA damage signaling and repair. In the present study, the time-correlated relationship between protein entrapment in pADPr-containing complexes and pADPr dynamics was further investigated using a combination of quantitative proteomics techniques. Despite intrinsic differences between spectral counting, SILAC and iTRAQ methodologies, we identified several proteins whose abundance was consistently correlated to pADPr levels.

It has been known for a long time that pADPr levels are transient and spontaneously resolving after their rapid degradation by PARG. However, there is an apparent gap between our understanding of the initial pADPr-associated molecular events underlying DDR and major nuclear reorganization, and the profound impact of pADPr on cell fate. In our study of pADPr dynamics, we found that several DDR factors are co-eluting with pADPr, consistent with the accumulation of DNA repair factors near the damage site and the current model where pADPr is viewed as a loading platform for the repair machinery (3,19). The recent identification of chromatin-associated proteins whose recruitment to DNA damage sites is pADPr-dependent [e.g.: CHD4 (38,73), MTA1(73), MRE11(74), NBS1(74), ALC1(39,40), APLF (75,76), XRCC1 (68), BMI-1 (77), MEL-18 (73)] also points towards this model. Thus, local poly(ADP-ribosyl)-ation at DNA damage sites may be a common phenomenon for the recruitment of DDR factors that control genome integrity. It is highly likely that more DDR factors and chromatin remodelers found in this study will join this expanding group of proteins.

Using laser micro-irradiation and live cell imaging analyses, we have shown that the retention of repair factors at sites of DNA damage can exhibit a wide range of dependency on pADPr. Given that pADPr formation can be subjected to a 100-fold increase after the induction of DNA damage (89), a rapid accumulation at the DNA damage site would logically occur for a non-covalent pADPr-binding protein. Indeed, we showed that XRCC1, which possesses a pADPr-binding motif (12), and CHFR, a PBZ-containing protein, are both showing a very significant decrease of retention at DNA damage sites when poly(ADP-ribosyl)ation is inhibited. There are a variety of intricate DNA damage response mechanisms that underlie spatial relocation of proteins at DNA breaks. Although poly(ADP-ribosyl)ation appears as the main driving force behind the recruitment of BER factors at DNA damage sites (i.e. XRCC1 and LIG3), this phenomenon is likely to be involved in the regulation of other functions as in the case of NHEJ. The identification of PARP-1, DNA-PK and KU70/80 as predominant pADPr-associated protein components suggest that these proteins participate to a same pathway to cope with DNA damage. This finding supports previous studies that established KU70, KU80 and DNA-PK as substrates of PARP-1 (78–80) and is also consistent with a model where PARP-1/DNA-PK interplay dictates the functional properties of the NHEJ repair complex (81). Although the relocation of core NHEJ factors at DNA damage sites is pADPr-independent, the presence of PARP-1 and pADPr in these complexes appears to play a more downstream role in the DNA damage response. This can be illustrated by reports indicating that poly(ADP-ribosyl)ation of the KU70/KU80 complex impairs its ability to bind DNA (78) or the stimulation of DNA-PK activity upon poly(ADP-ribosyl)ation (82). A recent study reports that PARP-1 binding to DSBs elicits substantial conformational changes in the DNA-PK dimer assembly (81). Following the idea that interactions within a PARP-1/DNA-PK complex might affect the mechanism of DNA-PK activation, the presence of pADPr through automodified PARP-1 could led to structural transitions with functional consequences on NHEJ.

This study and most of the current research focus on poly(ADP-ribosyl)ation as an early response to genotoxic stress. However, it is clear that the consequences of poly(ADP-ribosyl)ation are not limited to the early

DNA damage response, but also impact on stress response and cytoprotection. Later consequences may include changes in gene expression and global cellular responses of death and survival within hours and days (83).

This effort represents the most extensive proteomics coverage in the context of PARP activation following DNA damage and contributes to a growing body of evidence that implicates pADPr as a coordinator of multiple activities required for maintaining genome integrity.

SUPPLEMENTARY DATA

Supplementary Data are available at NAR Online: Supplementary Tables 1–5, Supplementary Methods and Supplementary References [84–89].

ACKNOWLEDGEMENTS

The authors are grateful to Dr Michèle Rouleau for useful discussions and suggestions for experiments, and Pierre Gagné for his assistance with network modeling and data processing. The authors also thank the University of British Columbia Proteomics Core Facility for the preparation and analysis of protein samples for SILAC analysis. We are particularly grateful to Dr Sylvie Bourassa who managed most of the samples at the Proteomics Platform of the Quebec Genomics Center and Sandra Breuils-Bonnet for iTRAQ labeling and IEF fractionation.

FUNDING

Canadian Institutes for Health Research [CIHR MOP-14052, MOP-74648]. Funding for open access charge: Canadian Institutes of Health Research (CIHR).

Conflict of interest statement. None declared.

REFERENCES

1. Tartier,L., Spenlehauer,C., Newman,H.C., Folkard,M., Prise,K.M., Michael,B.D., Menissier-de Murcia,J. and de Murcia,G. (2003) Local DNA damage by proton microbeam irradiation induces poly(ADP-ribose) synthesis in mammalian cells. *Mutagenesis*, **18**, 411–416.
2. Rouleau,M., Aubin,R.A. and Poirier,G.G. (2004) Poly(ADP-ribosyl)ated chromatin domains: access granted. *J. Cell Sci.*, **117**, 815–825.
3. Malanga,M. and Althaus,F.R. (2005) The role of poly(ADP-ribose) in the DNA damage signaling network. *Biochem. Cell Biol.*, **83**, 354–364.
4. Till,S. and Ladurner,A.G. (2009) Sensing NAD metabolites through macro domains. *Front. Biosci.*, **14**, 3246–3258.
5. Ahel,I., Ahel,D., Matsusaka,T., Clark,A.J., Pines,J., Boulton,S.J. and West,S.C. (2008) Poly(ADP-ribose)-binding zinc finger motifs in DNA repair/checkpoint proteins. *Nature*, **451**, 81–85.
6. Aravind,L. (2001) The WWE domain: a common interaction module in protein ubiquitination and ADP ribosylation. *Trends Biochem. Sci.*, **26**, 273–275.
7. Zhang,Y., Liu,S., Mickanin,C., Feng,Y., Charlat,O., Michaud,G.A., Schirle,M., Shi,X., Hild,M., Bauer,A. *et al.* (2011) RNF146 is a poly(ADP-ribose)-directed E3 ligase that regulates axin degradation and Wnt signalling. *Nat. Cell Biol.*, **13**, 623–629.
8. Wang,Z., Michaud,G.A., Cheng,Z., Zhang,Y., Hinds,T.R., Fan,E., Cong,F. and Xu,W. (2012) Recognition of the iso-ADP-ribose moiety in poly(ADP-ribose) by WWE domains suggests a general mechanism for poly(ADP-ribosyl)ation-dependent ubiquitination. *Genes Dev.*, **26**, 235–240.
9. Pleschke,J.M., Kleczkowska,H.E., Strohm,M. and Althaus,F.R. (2000) Poly(ADP-ribose) binds to specific domains in DNA damage checkpoint proteins. *J. Biol. Chem.*, **275**, 40974–40980.
10. Althaus,F.R., Kleczkowska,H.E., Malanga,M., Muntener,C.R., Pleschke,J.M., Ebner,M. and Auer,B. (1999) Poly ADP-ribosylation: a DNA break signal mechanism. *Mol. Cell Biochem.*, **193**, 5–11.
11. Gagne,J.P., Isabelle,M., Lo,K.S., Bourassa,S., Hendzel,M.J., Dawson,V.L., Dawson,T.M. and Poirier,G.G. (2008) Proteome-wide identification of poly(ADP-ribose) binding proteins and poly(ADP-ribose)-associated protein complexes. *Nucleic Acids Res.*, **36**, 6959–6976.
12. Egloff,M.P., Malet,H., Putics,A., Heinonen,M., Dutartre,H., Frangeul,A., Gruez,A., Campanacci,V., Cambillau,C., Ziebuhr,J. *et al.* (2006) Structural and functional basis for ADP-ribose and poly(ADP-ribose) binding by viral macro domains. *J. Virol.*, **80**, 8493–8502.
13. Karras,G.I., Kustatscher,G., Buhecha,H.R., Allen,M.D., Pugieux,C., Sait,F., Bycroft,M. and Ladurner,A.G. (2005) The macro domain is an ADP-ribose binding module. *EMBO J.*, **24**, 1911–1920.
14. Dani,N., Stilla,A., Marchegiani,A., Tamburro,A., Till,S., Ladurner,A.G., Corda,D. and Di Girolamo,M. (2009) Combining affinity purification by ADP-ribose-binding macro domains with mass spectrometry to define the mammalian ADP-ribosyl proteome. *Proc. Natl Acad. Sci. USA*, **106**, 4243–4248.
15. Slade,D., Dunstan,M.S., Barkauskaite,E., Weston,R., Lafite,P., Dixon,N., Ahel,M., Leys,D. and Ahel,I. (2011) The structure and catalytic mechanism of a poly(ADP-ribose) glycohydrolase. *Nature*, **477**, 616–620.
16. Ji,Y. (2011) Noncovalent pADPr interaction with proteins and competition with RNA for binding to proteins. *Methods Mol. Biol.*, **780**, 83–91.
17. Malanga,M. and Althaus,F.R. (2011) Noncovalent protein interaction with poly(ADP-ribose). *Methods Mol. Biol.*, **780**, 67–82.
18. Gagne,J.P., Haince,J.F., Pic,E. and Poirier,G.G. (2011) Affinity-based assays for the identification and quantitative evaluation of noncovalent poly(ADP-ribose)-binding proteins. *Methods Mol. Biol.*, **780**, 93–115.
19. Hassa,P.O., Haenni,S.S., Elser,M. and Hottiger,M.O. (2006) Nuclear ADP-ribosylation reactions in mammalian cells: where are we today and where are we going? *Microbiol. Mol. Biol. Rev.*, **70**, 789–829.
20. Banath,J.P., Klokov,D., MacPhail,S.H., Banuelos,C.A. and Olive,P.L. (2010) Residual gammaH2AX foci as an indication of lethal DNA lesions. *BMC Cancer*, **10**, 4.
21. Artus,C., Boujrad,H., Bouharrour,A., Brunelle,M.N., Hoos,S., Yuste,V.J., Lenormand,P., Rousselle,J.C., Namane,A., England,P. *et al.* (2010) AIF promotes chromatinolysis and caspase-independent programmed necrosis by interacting with histone H2AX. *EMBO J.*, **29**, 1585–1599.
22. Haince,J.F., Ouellet,M.E., McDonald,D., Hendzel,M.J. and Poirier,G.G. (2006) Dynamic relocation of poly(ADP-ribose) glycohydrolase isoforms during radiation-induced DNA damage. *Biochim. Biophys. Acta*, **1763**, 226–237.
23. Patel,C.N., Koh,D.W., Jacobson,M.K. and Oliveira,M.A. (2005) Identification of three critical acidic residues of poly(ADP-ribose) glycohydrolase involved in catalysis: determining the PARG catalytic domain. *Biochem. J.*, **388**, 493–500.
24. Shah,G.M., Poirier,D., Duchaine,C., Brochu,G., Desnoyers,S., Lagueux,J., Verreault,A., Hoflack,J.C., Kirkland,J.B. and Poirier,G.G. (1995) Methods for biochemical study of poly(ADP-ribose) metabolism in vitro and in vivo. *Anal Biochem.*, **227**, 1–13.
25. Hennig,C. (2010) fpc: Flexible procedures for clustering, Rpackage version 2.0-2. http://CRAN.R-project.org/package=fpc.

26. Harsha,H.C., Molina,H. and Pandey,A. (2008) Quantitative proteomics using stable isotope labeling with amino acids in cell culture. *Nat. Protoc.*, **3**, 505–516.
27. Blagoev,B. and Mann,M. (2006) Quantitative proteomics to study mitogen-activated protein kinases. *Methods*, **40**, 243–250.
28. Huang da,W., Sherman,B.T. and Lempicki,R.A. (2009) Systematic and integrative analysis of large gene lists using DAVID bioinformatics resources. *Nat. Protoc.*, **4**, 44–57.
29. Shannon,P., Markiel,A., Ozier,O., Baliga,N.S., Wang,J.T., Ramage,D., Amin,N., Schwikowski,B. and Ideker,T. (2003) Cytoscape: a software environment for integrated models of biomolecular interaction networks. *Genome Res.*, **13**, 2498–2504.
30. Maere,S., Heymans,K. and Kuiper,M. (2005) BiNGO: a Cytoscape plugin to assess overrepresentation of gene ontology categories in biological networks. *Bioinformatics*, **21**, 3448–3449.
31. Gao,J., Ade,A.S., Tarcea,V.G., Weymouth,T.E., Mirel,B.R., Jagadish,H.V. and States,D.J. (2009) Integrating and annotating the interactome using the MiMI plugin for cytoscape. *Bioinformatics*, **25**, 137–138.
32. Martin,A., Ochagavia,M.E., Rabasa,L.C., Miranda,J., Fernandez-de-Cossio,J. and Bringas,R. (2010) BisoGenet: a new tool for gene network building, visualization and analysis. *BMC Bioinformatics*, **11**, 91.
33. Gagne,J.P., Moreel,X., Gagne,P., Labelle,Y., Droit,A., Chevalier-Pare,M., Bourassa,S., McDonald,D., Hendzel,M.J., Prigent,C. *et al.* (2009) Proteomic investigation of phosphorylation sites in poly(ADP-ribose) polymerase-1 and poly(ADP-ribose) glycohydrolase. *J. Proteome Res.*, **8**, 1014–1029.
34. Haince,J.F., McDonald,D., Rodrigue,A., Dery,U., Masson,J.Y., Hendzel,M.J. and Poirier,G.G. (2008) PARP1-dependent kinetics of recruitment of MRE11 and NBS1 proteins to multiple DNA damage sites. *J. Biol. Chem.*, **283**, 1197–1208.
35. Kawamitsu,H., Hoshino,H., Okada,H., Miwa,M., Momoi,H. and Sugimura,T. (1984) Monoclonal antibodies to poly(adenosine diphosphate ribose) recognize different structures. *Biochemistry*, **23**, 3771–3777.
36. Hassler,M., Jankevicius,G. and Ladurner,A.G. (2011) PARG: a macrodomain in disguise. *Structure*, **19**, 1351–1353.
37. Allen,M.D., Buckle,A.M., Cordell,S.C., Lowe,J. and Bycroft,M. (2003) The crystal structure of AF1521 a protein from *Archaeoglobus fulgidus* with homology to the non-histone domain of macroH2A. *J. Mol. Biol.*, **330**, 503–511.
38. Polo,S.E., Kaidi,A., Baskcomb,L., Galanty,Y. and Jackson,S.P. (2010) Regulation of DNA-damage responses and cell-cycle progression by the chromatin remodelling factor CHD4. *EMBO J.*, **29**, 3130–3139.
39. Ahel,D., Horejsi,Z., Wiechens,N., Polo,S.E., Garcia-Wilson,E., Ahel,I., Flynn,H., Skehel,M., West,S.C., Jackson,S.P. *et al.* (2009) Poly(ADP-ribose)-dependent regulation of DNA repair by the chromatin remodeling enzyme ALC1. *Science*, **325**, 1240–1243.
40. Gottschalk,A.J., Timinszky,G., Kong,S.E., Jin,J., Cai,Y., Swanson,S.K., Washburn,M.P., Florens,L., Ladurner,A.G., Conaway,J.W. *et al.* (2009) Poly(ADP-ribosyl)ation directs recruitment and activation of an ATP-dependent chromatin remodeler. *Proc. Natl Acad. Sci. USA*, **106**, 13770–13774.
41. Fahrer,J., Popp,O., Malanga,M., Beneke,S., Markovitz,D.M., Ferrando-May,E., Burkle,A. and Kappes,F. (2010) High-affinity interaction of poly(ADP-ribose) and the human DEK oncoprotein depends upon chain length. *Biochemistry*, **49**, 7119–7130.
42. Chang,W., Dynek,J.N. and Smith,S. (2005) NuMA is a major acceptor of poly(ADP-ribosyl)ation by tankyrase 1 in mitosis. *Biochem. J.*, **391**, 177–184.
43. Kickhoefer,V.A., Siva,A.C., Kedersha,N.L., Inman,E.M., Ruland,C., Streuli,M. and Rome,L.H. (1999) The 193-kD vault protein, VPARP, is a novel poly(ADP-ribose) polymerase. *J. Cell Biol.*, **146**, 917–928.
44. Saxena,A., Saffery,R., Wong,L.H., Kalitsis,P. and Choo,K.H. (2002) Centromere proteins Cenpa, Cenpb, and Bub3 interact with poly(ADP-ribose) polymerase-1 protein and are poly(ADP-ribosyl)ated. *J. Biol. Chem.*, **277**, 26921–26926.
45. Ruscetti,T., Lehnert,B.E., Halbrook,J., Le Trong,H., Hoekstra,M.F., Chen,D.J. and Peterson,S.R. (1998) Stimulation of the DNA-dependent protein kinase by poly(ADP-ribose) polymerase. *J. Biol. Chem.*, **273**, 14461–14467.
46. Reale,A., Matteis,G.D., Galleazzi,G., Zampieri,M. and Caiafa,P. (2005) Modulation of DNMT1 activity by ADP-ribose polymers. *Oncogene*, **24**, 13–19.
47. Huang,J.Y., Chen,W.H., Chang,Y.L., Wang,H.T., Chuang,W.T. and Lee,S.C. (2006) Modulation of nucleosome-binding activity of FACT by poly(ADP-ribosyl)ation. *Nucleic Acids Res.*, **34**, 2398–2407.
48. Malanga,M. and Althaus,F.R. (2004) Poly(ADP-ribose) reactivates stalled DNA topoisomerase I and induces DNA strand break resealing. *J. Biol. Chem.*, **279**, 5244–5248.
49. Meyer-Ficca,M.L., Lonchar,J.D., Ihara,M., Meistrich,M.L., Austin,C.A. and Meyer,R.G. (2011) Poly(ADP-Ribose) polymerases PARP1 and PARP2 modulate topoisomerase II beta (TOP2B) function during chromatin condensation in mouse spermiogenesis. *Biol. Reprod.*, **84**, 900–909.
50. Gagne,J.P., Hunter,J.M., Labrecque,B., Chabot,B. and Poirier,G.G. (2003) A proteomic approach to the identification of heterogeneous nuclear ribonucleoproteins as a new family of poly(ADP-ribose)-binding proteins. *Biochem. J.*, **371**, 331–340.
51. Ji,Y. and Tulin,A.V. (2009) Poly(ADP-ribosyl)ation of heterogeneous nuclear ribonucleoproteins modulates splicing. *Nucleic Acids Res.*, **37**, 3501–3513.
52. Panzeter,P.L., Zweifel,B., Malanga,M., Waser,S.H., Richard,M. and Althaus,F.R. (1993) Targeting of histone tails by poly(ADP-ribose). *J. Biol. Chem.*, **268**, 17662–17664.
53. Wang,Y., Kim,N.S., Haince,J.F., Kang,H.C., David,K.K., Andrabi,S.A., Poirier,G.G., Dawson,V.L. and Dawson,T.M. (2011) Poly(ADP-ribose) (PAR) binding to apoptosis-inducing factor is critical for PAR polymerase-1-dependent cell death (parthanatos). *Sci. Signal*, **4**, ra20.
54. Slama,J.T., Aboul-Ela,N., Goli,D.M., Cheesman,B.V., Simmons,A.M. and Jacobson,M.K. (1995) Specific inhibition of poly(ADP-ribose) glycohydrolase by adenosine diphosphate (hydroxymethyl)pyrrolidinediol. *J. Med. Chem.*, **38**, 389–393.
55. Malanga,M. and Althaus,F.R. (1994) Poly(ADP-ribose) molecules formed during DNA repair in vivo. *J. Biol. Chem.*, **269**, 17691–17696.
56. D'Amours,D., Desnoyers,S., D'Silva,I. and Poirier,G.G. (1999) Poly(ADP-ribosyl)ation reactions in the regulation of nuclear functions. *Biochem. J.*, **342 (Pt 2)**, 249–268.
57. Leppard,J.B., Dong,Z., Mackey,Z.B. and Tomkinson,A.E. (2003) Physical and functional interaction between DNA ligase IIIalpha and poly(ADP-Ribose) polymerase 1 in DNA single-strand break repair. *Mol. Cell. Biol.*, **23**, 5919–5927.
58. Schulze,W.X. and Usadel,B. (2010) Quantitation in mass-spectrometry-based proteomics. *Annu. Rev. Plant Biol.*, **61**, 491–516.
59. Mallick,P. and Kuster,B. (2010) Proteomics: a pragmatic perspective. *Nat. Biotechnol.*, **28**, 695–709.
60. Ong,S.E., Blagoev,B., Kratchmarova,I., Kristensen,D.B., Steen,H., Pandey,A. and Mann,M. (2002) Stable isotope labeling by amino acids in cell culture, SILAC, as a simple and accurate approach to expression proteomics. *Mol. Cell. Proteomics*, **1**, 376–386.
61. Ross,P.L., Huang,Y.N., Marchese,J.N., Williamson,B., Parker,K., Hattan,S., Khainovski,N., Pillai,S., Dey,S., Daniels,S. *et al.* (2004) Multiplexed protein quantitation in *Saccharomyces cerevisiae* using amine-reactive isobaric tagging reagents. *Mol. Cell. Proteomics.*, **3**, 1154–1169.
62. Montes de Oca,R., Shoemaker,C.J., Gucek,M., Cole,R.N. and Wilson,K.L. (2009) Barrier-to-autointegration factor proteome reveals chromatin-regulatory partners. *PLoS One*, **4**, e7050.
63. Yang,X., Zou,P., Yao,J., Yun,D., Bao,H., Du,R., Long,J. and Chen,X. (2010) Proteomic dissection of cell type-specific H2AX-interacting protein complex associated with hepatocellular carcinoma. *J. Proteome Res.*, **9**, 1402–1415.
64. Hassa,P.O., Haenni,S.S., Buerki,C., Meier,N.I., Lane,W.S., Owen,H., Gersbach,M., Imhof,R. and Hottiger,M.O. (2005) Acetylation of poly(ADP-ribose) polymerase-1 by p300/CREB-binding protein regulates coactivation of NF-kappaB-dependent transcription. *J. Biol. Chem.*, **280**, 40450–40464.
65. Eustermann,S., Brockmann,C., Mehrotra,P.V., Yang,J.C., Loakes,D., West,S.C., Ahel,I. and Neuhaus,D. (2010) Solution structures of the two PBZ domains from human APLF and their interaction with poly(ADP-ribose). *Nat. Struct. Mol. Biol.*, **17**, 241–243.

66. Li,G.Y., McCulloch,R.D., Fenton,A.L., Cheung,M., Meng,L., Ikura,M. and Koch,C.A. (2010) Structure and identification of ADP-ribose recognition motifs of APLF and role in the DNA damage response. *Proc. Natl Acad. Sci. USA*, **107**, 9129–9134.
67. Malanga,M. and Althaus,F.R. (2005) The role of poly(ADP-ribose) in the DNA damage signaling network. *Biochem. Cell Biol.*, **83**, 354–364.
68. El-Khamisy,S.F., Masutani,M., Suzuki,H. and Caldecott,K.W. (2003) A requirement for PARP-1 for the assembly or stability of XRCC1 nuclear foci at sites of oxidative DNA damage. *Nucleic Acids Res.*, **31**, 5526–5533.
69. Masson,M., Niedergang,C., Schreiber,V., Muller,S., Menissier-de Murcia,J. and de Murcia,G. (1998) XRCC1 is specifically associated with poly(ADP-ribose) polymerase and negatively regulates its activity following DNA damage. *Mol. Cell. Biol.*, **18**, 3563–3571.
70. Mortusewicz,O., Ame,J.C., Schreiber,V. and Leonhardt,H. (2007) Feedback-regulated poly(ADP-ribosyl)ation by PARP-1 is required for rapid response to DNA damage in living cells. *Nucleic Acids Res.*, **35**, 7665–7675.
71. Rouleau,M., Patel,A., Hendzel,M.J., Kaufmann,S.H. and Poirier,G.G. (2010) PARP inhibition: PARP1 and beyond. *Nat. Rev. Cancer*, **10**, 293–301.
72. Wu,J., Chen,Y., Lu,L.Y., Wu,Y., Paulsen,M.T., Ljungman,M., Ferguson,D.O. and Yu,X. (2011) Chfr and RNF8 synergistically regulate ATM activation. *Nat. Struct. Mol. Biol.*, **18**, 761–768.
73. Chou,D.M., Adamson,B., Dephoure,N.E., Tan,X., Nottke,A.C., Hurov,K.E., Gygi,S.P., Colaiacovo,M.P. and Elledge,S.J. (2010) A chromatin localization screen reveals poly (ADP ribose)-regulated recruitment of the repressive polycomb and NuRD complexes to sites of DNA damage. *Proc. Natl Acad. Sci. USA*, **107**, 18475–18480.
74. Haince,J.F., McDonald,D., Rodrigue,A., Dery,U., Masson,J.Y., Hendzel,M.J. and Poirier,G.G. (2008) PARP1-dependent kinetics of recruitment of MRE11 and NBS1 proteins to multiple DNA damage sites. *J. Biol. Chem.*, **283**, 1197–1208.
75. Harris,J.L., Jakob,B., Taucher-Scholz,G., Dianov,G.L., Becherel,O.J. and Lavin,M.F. (2009) Aprataxin, poly-ADP ribose polymerase 1 (PARP-1) and apurinic endonuclease 1 (APE1) function together to protect the genome against oxidative damage. *Hum. Mol. Genet.*, **18**, 4102–4117.
76. Rulten,S.L., Cortes-Ledesma,F., Guo,L., Iles,N.J. and Caldecott,K.W. (2008) APLF (C2orf13) is a novel component of poly(ADP-ribose) signaling in mammalian cells. *Mol. Cell Biol.*, **28**, 4620–4628.
77. Gieni,R.S., Ismail,I.H., Campbell,S. and Hendzel,M.J. (2011) Polycomb group proteins in the DNA damage response-A link between radiation resistance and "stemness". *Cell Cycle*, **10**, 883–894.
78. Li,B., Navarro,S., Kasahara,N. and Comai,L. (2004) Identification and biochemical characterization of a Werner's syndrome protein complex with Ku70/80 and poly(ADP-ribose) polymerase-1. *J. Biol. Chem.*, **279**, 13659–13667.
79. Galande,S. and Kohwi-Shigematsu,T. (1999) Poly(ADP-ribose) polymerase and Ku autoantigen form a complex and synergistically bind to matrix attachment sequences. *J. Biol. Chem.*, **274**, 20521–20528.
80. Ariumi,Y., Masutani,M., Copeland,T.D., Mimori,T., Sugimura,T., Shimotohno,K., Ueda,K., Hatanaka,M. and Noda,M. (1999) Suppression of the poly(ADP-ribose) polymerase activity by DNA-dependent protein kinase in vitro. *Oncogene*, **18**, 4616–4625.
81. Spagnolo,L., Barbeau,J., Curtin,N.J., Morris,E.P. and Pearl,L.H. (2012) Visualization of a DNA-PK/PARP1 complex. *Nucleic Acids Res.*, **40**, 4168–4177.
82. Ruscetti,T., Lehnert,B.E., Halbrook,J., Le Trong,H., Hoekstra,M.F., Chen,D.J. and Peterson,S.R. (1998) Stimulation of the DNA-dependent protein kinase by poly(ADP-ribose) polymerase. *J. Biol. Chem.*, **273**, 14461–14467.
83. Schmidt-Ullrich,R.K. (2003) Molecular targets in radiation oncology. *Oncogene*, **22**, 5730–5733.
84. Keller,A., Nesvizhskii,A.I., Kolker,E. and Aebersold,R. (2002) Empirical statistical model to estimate the accuracy of peptide identifications made by MS/MS and database search. *Anal Chem.*, **74**, 5383–5392.
85. Nesvizhskii,A.I., Keller,A., Kolker,E. and Aebersold,R. (2003) A statistical model for identifying proteins by tandem mass spectrometry. *Anal Chem.*, **75**, 4646–4658.
86. Shilov,I.V., Seymour,S.L., Patel,A.A., Loboda,A., Tang,W.H., Keating,S.P., Hunter,C.L., Nuwaysir,L.M. and Schaeffer,D.A. (2007) The Paragon Algorithm, a next generation search engine that uses sequence temperature values and feature probabilities to identify peptides from tandem mass spectra. *Mol. Cell. Proteomics*, **6**, 1638–1655.
87. Ishihama,Y., Rappsilber,J. and Mann,M. (2006) Modular stop and go extraction tips with stacked disks for parallel and multidimensional Peptide fractionation in proteomics. *J. Proteome Res.*, **5**, 988–994.
88. Chan,Q.W., Howes,C.G. and Foster,L.J. (2006) Quantitative comparison of caste differences in honeybee hemolymph. *Mol. Cell. Proteomics*, **5**, 2252–2262.
89. Gao,J., Ade,A.S., Tarcea,V.G., Weymouth,T.E., Mirel,B.R., Jagadish,H.V. and States,D.J. (2009) Integrating and annotating the interactome using the MiMI plugin for cytoscape. *Bioinformatics*, **25**, 137–138.